Dissection of GTPase activating proteins reveals functional asymmetry in the COPI coat

Eric C. Arakel [1], Martina Huranova [§,2,3], Alejandro F. Estrada [§,2], E-Ming Rau [2], Anne Spang [2,*] and Blanche Schwappach [1,4*]

[1] Department of Molecular Biology, Universitätsmedizin Göttingen, Humboldtallee 23, 37073 Göttingen, Germany

[2] Growth and Development, Biozentrum, University of Basel, Basel, Switzerland

[3] Laboratory of Adaptive Immunity, Institute of Molecular Genetics of the Czech Academy of Sciences, Prague, Czech Republic

[4] Max-Planck Institute for Biophysical Chemistry, 37077 Göttingen, Germany

[§] These authors contributed equally

[*] correspondence: anne.spang@unibas.ch (AS); blanche.schwappach@med.uni-goettingen.de (BS)

Blanche Schwappach
Tel.: +49 551 395961
Fax: +49 551 395960

Keywords: AMP kinase, Arf GTPase, ArfGAP, COPI vesicle, Gcs1, Glo3

Summary statement: The regulatory domain of the COPI-associated ArfGAP Glo3 can stabilize the COPI coat. GTP hydrolysis is necessary to resolve the stabilized state. This mechanism is regulated by phosphorylation.

Abstract

The Arf GTPase controls formation of the COPI vesicle coat. Recent structural models of COPI revealed the positioning of two Arf1 molecules in contrasting molecular environments. Each of these pockets for Arf1 is expected to also accommodate an Arf GTPase-activating protein (ArfGAP). Structural evidence and protein interactions observed between isolated domains indirectly suggests that each niche may preferentially recruit one of the two ArfGAPs known to affect COPI, Gcs1/ArfGAP1 and Glo3/ArfGAP2/3, although only partial structures are available. The functional role of the unique non-catalytic domain of either ArfGAP has not been integrated into the current COPI structural model. Here, we delineate key differences in the consequences of triggering GTP hydrolysis via the activity of one versus the other ArfGAP. We demonstrate that Glo3/ArfGAP2/3 specifically triggers Arf1 GTP hydrolysis impinging on the stability of the COPI coat. We show that the yeast homologue of AMP kinase, Snf1, phosphorylates the region of Glo3 that is critical for this effect and thereby regulates its function in the COPI-vesicle cycle. Our results revise the model of ArfGAP function in the molecular context of COPI.

Introduction

Coated vesicles transport proteins and lipids between compartments of the secretory pathway. Coats are macromolecular assemblies that associate with membranes, selectively capture proteins and lipids, deform the underlying membrane to form vesicles, and help accurately target these vesicles to their physiological destinations.

The COPI coat is formed by an obligate heptamer – also termed coatomer – consisting of the α, β', ε, β, γ, δ, and ζ subunits. Coatomer is recruited *en-bloc* to membranes (Hara-Kuge et al., 1994). Fundamentally, the COPI coat mediates the retrograde trafficking of proteins and lipids from the Golgi to the ER and within intra-Golgi compartments (Arakel et al., 2016; Beck et al., 2009; Pellett et al., 2013; Spang and Schekman, 1998). Several reports have also implicated COPI in endosomal recycling and regulating lipid droplet homeostasis (Aniento et al., 1996; Beller et al., 2008; Xu et al., 2017).

Activation of the small GTPase Arf1 and its subsequent membrane anchoring, via the exchange of GDP for GTP by a guanine nucleotide exchange factor (GEF), promotes the recruitment of coatomer to membranes (Antonny et al., 1997; Yu et al., 2012). Two COPI-associated Arf1 GTPase activating proteins (GAPs), ArfGAP1 and ArfGAP2/3 and their yeast homologues Gcs1 and Glo3, stimulate GTP hydrolysis in Arf1 (Spang et al., 2010; Weimer et al., 2008) (Fig. 1A and 1B). Inhibition of GTP hydrolysis results in deficient sorting and the accumulation of COPI on the membrane (Lanoix et al., 1999; Nickel et al., 1998; Presley et al., 2002; Tanigawa et al., 1993). Hence, GTP hydrolysis in Arf1 is thought to be bi-functional, effecting efficient cargo capture and vesicle uncoating.

Both ArfGAPs contain an evolutionarily conserved catalytic zinc finger domain while their non-catalytical domains are structurally unrelated (Randazzo and Hirsch, 2004; Schindler et al., 2009; Spang et al., 2010). Why COPI relies on more than one ArfGAP is a mystery. There is circumstantial evidence suggesting that Gcs1/ArfGAP1 and Glo3/ArfGAP2/3 fulfil different functions in the COPI vesicle cycle, yet the precise role of either ArfGAP remains elusive (Poon et al., 1999; Poon et al., 2001; Schindler and Spang, 2007; Schindler et al., 2009). Curiously, as opposed to many other GAPs and effectors of GTPases, COPI and ArfGAP do not compete for access to Arf1. Instead, all three exist in one complex, and the activity of either ArfGAP is significantly enhanced in the presence of COPI (Szafer et al., 2001; Weimer et al., 2008). A series of primarily *in vitro* reconstitution assays have helped to elucidate the intricacies of this process, unequivocally demonstrating that both ArfGAP1 and ArfGAP2 can initiate COPI vesicle uncoating (Weimer et al., 2008).

However, little is known about the precise orchestration of GTP-hydrolysis in Arf1, which governs COPI function. The specific roles of the two COPI-associated ArfGAPs, which drive GTP hydrolysis in Arf1, remain unresolved due to their overlapping basic function, endowed by the highly conserved ArfGAP domain (Poon et al., 1999). Recent structural models of COPI, based on cryo-EM tomography (Bykov et al., 2017; Dodonova et al., 2017), have shed light on the complex interplay of proteins involved in the COPI vesicle cycle and now offer structurally motivated hypotheses to resolve these issues. Harnessing recent structural information in an *in vivo* dissection, we now demonstrate that the activity of both ArfGAPs and the subsequent GTP-hydrolysis in Arf1 effect distinct cellular processes despite the fact that their basic ArfGAP activities can substitute for each other since yeast strains

lacking one or the other can survive. Our dissection pinpoints key differences between the ArfGAPs and their spatially segregated regulation of Arf1. We also identify a novel phospho-regulatory mechanism that potentially serves as a molecular timer on the ArfGAP controlling basic aspects of COPI coat turnover. We provide a model, which solves the conundrum of the seemingly redundant functions of the ArfGAPs. Furthermore, we assign roles to each ArfGAP that fit the molecular environment in which they exist in COPI.

Results

Glo3, not Gcs1, is stably associated with COPI.

The two ArfGAPs, Glo3/ArfGAP2/3 and Gcs1/ArfGAP1 regulate COPI function in yeast (Poon et al., 1999). Early studies implicated ArfGAP1 as the relevant GAP and proposed ArfGAP1 as a functional component of the coat (Yang et al., 2002). Others have demonstrated that COPI also associates with ArfGAP2/Glo3 (Frigerio et al., 2007; Lewis et al., 2004). Elucidation of the structure of the COPI coat on reconstituted vesicles (Dodonova et al., 2017; Dodonova et al., 2015) and insights into the molecular interactions of either ArfGAP with coatomer (Rawet et al., 2010; Schindler et al., 2009; Suckling et al., 2014; Watson et al., 2004) leads to the hypothesis that they exist in contrasting molecular environments (Fig. 1A), just like the two Arf1 GTPase molecules associated with the coat (Dodonova et al., 2017). Interestingly, this hypothesis and a structure encompassing the ArfGAP domain of Glo3/ArfGAP2/3 (Dodonova et al., 2017) predicts that this ArfGAP occupies a niche where three Glo3/ArfGAP2/3 molecules come into close proximity at the center of a COPI triad (Fig. 1B).

Based on the different binding parameters of the molecular interactions underlying this hypothesis (Pevzner et al., 2012; Suckling et al., 2014; Watson et al., 2004), we expected to observe differences in how stably the two yeast ArfGAPs interact with COPI and tested this hypothesis by affinity purification. Enrichment of GFP-tagged Glo3 or Gcs1 from cytosol (Fig. 1C) or from detergent extracts (Fig. 1D and 1E) revealed that in contrast to Gcs1, COPI is strongly associated with Glo3, the yeast homolog of ArfGAP2/3. A number of other proteins that interact with COPI such as the Erv41-46 complex (Rhiel et al., 2018; Shibuya et al., 2015), the yeast homologue of ERGIC 2/3, specifically co-purified with Glo3 (Fig. 1E, Appendix Table S3). This suggests that COPI and Glo3, but not Gcs1, are in a stable complex.

Glo3 binds COPI via the γ-COP appendage domain (Pevzner et al., 2012; Watson et al., 2004) and occupies a niche adjacent to Arf1 created by the polymerising coat (Dodonova et al., 2017). Gcs1 binds the μ-homology domain (μHD) of δ-COP via a C-terminal δL/ tryptophan-based motif (Cosson et al., 1998; Rawet et al., 2010; Suckling et al., 2014). Binding affinities of the δ-COP μHD for peptides containing the tryptophan motif were reported to be in the low micromolar range (Suckling et al., 2014), possibly explaining why the COPI coat does not co-purify with Gcs1 (Fig. 1C, 1D, 1E).

The stable association between Glo3 and COPI maps to a unique domain of Glo3.

To test whether the stable association between Glo3 and COPI was due to direct binding, we reconstituted the interaction from purified components. We recombinantly expressed Glo3, lacking a C-terminal amphipathic helix to aid protein

solubility, and found it to associate stoichiometrically with coatomer purified from *S. cerevisiae* (Fig. 2A).

Truncations of Glo3 were designed to reassess which domains of Glo3 are necessary and sufficient for the stable association of Glo3 and COPI (Schindler et al., 2009). Binding experiments with partial constructs of Glo3 containing the GAP domain and the Binding of Coatomer, Cargo and SNARE (BoCCS) domain, the BoCCS alone (137-375), the BoCCS and the evolutionarily conserved Glo3-regulatory motif (GRM), or the GRM alone clearly revealed that the BoCCS domain of Glo3 is crucial to bind coatomer directly (Fig. 2B and 2C). A construct (296-459) lacking a stretch of positively charged residues in the BoCCS attributed to mediate COPI binding (Kliouchnikov et al., 2008; Schindler et al., 2009), did not bind COPI. Similarly, a charge reversal of the same positively charged residues in the Glo3 BoCCS domain, to negatively charged glutamic acid residues, resulted in a loss of COPI binding (Fig. S1A). Glo3 and its mammalian homologues contain a highly conserved tandem repeat of an ISSxxxFG sequence (Yahara et al., 2006) and this GRM motif regulates the function of Glo3 (Schindler et al., 2009). Our binding data show that the GRM domain alone is not sufficient to confer a stable interaction between Glo3 and COPI. More generally, the direct and robust association of COPI and Glo3 raises the possibility that Glo3 fulfills an additional function beyond its recognised role in GTP-hydrolysis.

GAP action on β- and γ-Arf1 is functionally distinct.

The intrinsic GTPase activity of Arf1 is negligible and requires an ArfGAP to catalyse GTP-hydrolysis (Kahn and Gilman, 1986; Randazzo and Kahn, 1994). Neither ArfGAP is essential in either yeast or mammals implying a certain degree of functional redundancy. However, the combined deletion of both causes lethality (Frigerio et al., 2007; Poon et al., 1999).

Arf1 binds virtually equivalent sites on the homologous β- and γ-COP subunits (Yu et al., 2012). However, in the recently elucidated structural context of the membrane-associated COPI coat, β- and γ-Arf1 (denominated by the bound COPI subunit) occupy structurally distinct molecular environments within the coat lattice (Dodonova et al., 2017) (Fig. 1A and 1B). The GAP domain of ArfGAP2 was observed positioned only near γ-Arf1 and not β-Arf1 (Dodonova et al., 2017). Taking into consideration the positional restrictions imposed by the flexible, interacting domains of δ- and γ-COP, it is tempting to speculate that ArfGAP1/Gcs1 is positioned near β-Arf1.

It remains unclear how the respective position of either Arf1 molecule, and by extension, of either ArfGAP, affects their function in the COPI vesicle cycle. The different molecular environments as well as the presence of non-conserved C-terminal domains in the ArfGAPs suggest distinct functions, which are mechanistically unexplored.

To unravel these distinct functions, we first sought to inhibit the most highly conserved domain between Glo3 and Gcs1. The GAP domain of Glo3 and Gcs1 contains a highly conserved arginine residue (R54 in Gcs1 and R59 in Glo3). This arginine finger is essential for GAP function. Mutation of the arginine to a lysine dramatically impairs the GAP activity of both Gcs1 and Glo3 (Lewis et al., 2004; Yanagisawa et al., 2002). These dominant negative forms of either ArfGAP fill their respective niches unproductively. Expression of the GAP-dead mutants in strains of their respective deletion backgrounds (i.e. expression of Glo3 R59K in Δ*glo3* and Gcs1 R54K in Δ*gcs1* strains) resulted in remarkably distinct phenotypes (Fig. 3). Cells harbouring the Gcs1 GAP-dead mutant were viable (Fig. 3A) while expression of the GAP-dead Glo3 caused lethality (Fig. 3B). All proteins were expressed to high

steady-state protein levels (Fig. 3C) excluding the lack of expression as a trivial explanation for the cell's ability to tolerate the GAP-dead Gcs1.

Only a minor decrease in growth rate was observed in GAP-dead Gcs1 expressing cells. To test whether this effect was COPI-related we compared variants of GAP-dead Gcs1 that affected membrane recruitment or COPI interaction. We introduced a mutation in the ALPS motif (L246D) that disrupts it and impairs the recruitment of Gcs1 to the membrane (Bigay et al., 2005; Xu et al., 2013). Similarly, we introduced a substitution combining the replacement of the C-terminal tryptophan-motif (Rawet et al., 2010; Suckling et al., 2014) and three upstream phenylalanine residues, a manipulation expected to affect the binding of Gcs1 to δ-COP and to impair the targeting to its putative niche in the COPI coat. Both variants appeared to rescue the minor decline in growth (Fig. 3A).

We also investigated the molecular determinants of the toxic effects exerted by GAP-dead Glo3. The lethality caused by the expression of GAP-dead Glo3 was reversed either by the deletion of the GRM or the mutation of a stretch of positively charged residues (Δ2x+ve) in the BoCCS, previously ascribed to coordinate COPI binding (Kliouchnikov et al., 2008; Schindler et al., 2009), which is consistent with the direct binding data presented in Fig. 2 and Fig. S1A. Importantly, those GAP-dead variants that did not negatively affect growth were also expressed to high steady-state protein levels (Fig. 3C). In contrast, deletion of the conserved C-terminal amphipathic motif of Glo3, which governs the Golgi-localisation of ArfGAP3 (Kliouchnikov et al., 2008), was unable to reverse the dominant-negative lethality induced by GAP-dead Glo3 (Fig. 3B). Deletion of the C-terminal amphipathic helix of Glo3 did not cause a change in its steady-state subcellular localisation or its association with COPI (Fig. S2). Based on its strongly reduced association with

COPI (Fig. S1), the COPI-binding deficient mutant (Δ2x+ve) may fail to target GAP-dead Glo3 to the COPI coat, phenocopying Δ*glo3*. Cell viability upon deletion of the GRM domain in the GAP-dead mutant could either indicate a failed targeting of Glo3 to COPI or report on the influence of an intact GRM in executing GAP-domain function. The interaction between Glo3 ΔGRM and COPI was unaltered (Figs. 2B, S2A), in favor of the latter hypothesis.

This phenotypic difference in viability caused by the expression of either GAP-dead mutant indicates that locking γ-Arf1 in its GTP-bound state via catalytically inactive Glo3, but not β-Arf1 via catalytically inactive Gcs1, is detrimental to the cell, in turn implying that GTP-hydrolysis in either Arf1 triggers mechanistically distinct outcomes.

The Snf1/AMP-activated protein kinase phosphorylates the Glo3 motif.

Since it is the BoCCS and not the GRM motif that is responsible for the stable interaction between Glo3 and COPI, we next explored determinants of toxicity in the GRM motif of GAP-dead Glo3 (Fig. 4A). The GRM contains four predicted phosphorylation sites (S389, S398, S423, S424) (Blom et al., 1999). Sequential mutation of these residues identified two phosphosites within the GRM, S389 and S398 (Fig. 4B and S3). Affinity purification following stabilizing cross-linking led to the identification of Snf1 as the kinase phosphorylating S389 (Fig. 4B and Fig. S3A-E). The Snf1/AMP-activated protein kinase is a key sensor of cellular energy levels and plays a vital role in the subsequent adaptation to metabolic stress (Hardie et al., 1998). Indeed, Glo3 appeared heavily phosphorylated when cells were starved for glucose (Fig. 4C), a condition that strongly activates Snf1.

To test whether this condition and hence Snf1 activation affects the presence of Arf1 on Golgi membranes, we used fluorescence recovery after photobleaching (FRAP) to investigate the dissociation kinetics of Arf1-GFP from Golgi membranes as identified by the polytopic membrane protein Vrg4-mCherry (Fig. 4D). Interestingly, glucose starvation increased the dissociation of Arf1 from these membranes (k_{off} 0.234 s^{-1} versus 0.164 s^{-1}) and decreased the immobile fraction of Arf1-GFP (Table S4). Similarly, expression of a phosphomimetic mutant of Glo3 (S389,398D), which was designed to simulate glucose starvation, increased the dissociation of Arf1 from Golgi membranes (Fig 4E and Table S4). In contrast, expression of the S389,398A mutant of Glo3 led to a decrease in the dissociation of Arf1 from Golgi membranes. These results support the notion that COPI-dependent vesicular traffic is less active under conditions of glucose starvation, when the GRM domain of Glo3 is phosphorylated. We conclude that phosphorylation of Glo3 by Snf1 contributes to this regulation. In fact, Snf1 has previously been implicated in phosphorylating a number of proteins involved in vesicle trafficking, including Gcs1, Glo3 and Age2 (Braun et al., 2014). A study in HeLa cells also demonstrated that AMPK plays a crucial role in inhibiting vesicular transport pathways upon energy and nutrient starvation (Yang et al., 2018). Consistent with this study, we demonstrate that in addition to Glo3, the other ArfGAP Gcs1 also appears to be post-translationally modified upon glucose starvation, based on the observed electrophoretic migratory differences following SDS-PAGE (Fig 4C). However, for Glo3 a second serine – S398 was phosphorylated in the absence of Snf1 implicating a second unidentified kinase acting on this ArfGAP (Fig. 4B, Fig. S3C). These findings suggest that the regulation of Glo3 by phosphorylation of the GRM is complex.

Phosphorylation of the Glo3 motif regulates Glo3 function.

We hypothesized that regulation via the identified phosphosites might converge on the same crucial function that was revealed by the fact that the GRM was required to render a GAP-dead Glo3 toxic (Fig. 3B). Therefore, we combined the Glo3 (S389,398D) and the Glo3 (S389,398A) mutants with the catalytically inactive R59K substitution (Fig. 5A). Expression of the un-phosphorylated GAP-dead mutant caused lethality while the phospho-mimetic counteracts the dominant-negative lethality, supporting growth (Fig. 5A). All proteins were expressed to high steady-state protein levels (Fig. 5B). Thus, phosphorylation of the GRM, like deletion of the entire GRM, rescued the GAP-dead toxicity, indicating that phosphorylation inactivates the GRM.

Next, we tested the possibility that Glo3 binding of coatomer could also be regulated by phosphorylation of the GRM domain. In contrast to the mutation of a stretch of positively charged residues coordinating COPI binding via the BoCSS domain (Fig. 3B and Fig. S1A), which led to a loss of coatomer association with Glo3, both phospho-site variants and truncated Glo3, lacking its GRM, were found associated with COPI to a similar extent (Fig. 5C). These results rule out defective targeting of Glo3 to COPI as the basis of viability in the presence of the phospho-mimetic residues in the GRM domain (Fig. 5A). Instead, our findings implicate GRM regulation as a determinant of viability in cells expressing a catalytically inactive form of Glo3 (Fig. 5D). This would indicate that in the presence of a functional GRM domain, GTP-hydrolysis in γ-Arf1 is essential. It moreover suggests that the GRM domain senses conformational changes triggered by GTP-hydrolysis and its phosphorylation/ dephosphorylation status impinges on its functionality. In line with this conclusion, substitution of serine 389 to either alanine (constitutively un-

phosphorylated) or aspartic acid (phospho-mimetic) precluded the ability of wild-type Glo3 to suppress the growth phenotype of a COPI hypomorph (*sec26^FW^*) (Fig. S3F). This result suggests that robust COPI function under different growth conditions relies on the regulation of Glo3 by phosphorylation and dephosphorylation as expected for a reversible posttranslational modification.

Cargo sorting occurs in the molecular environment of β-Arf1.

Deletion of either Glo3 or Gcs1 is tolerated by yeast cells, indicating that the presence of one of the GAPs is sufficient to mediate COPI-dependent transport. Therefore, the question arises whether the model is correct that COPI associates with both ArfGAPs simultaneously. To test the model, we enriched Glo3-associated coat and probed for the presence of Gcs1 (Fig. 6A). Consistent with the low affinity of Gcs1 to the μ-homology domain of delta-COP (Suckling et al. 2014) no endogenous Gcs1 co-purified with Glo3. When overexpressed, Gcs1 weakly co-precipitated with Glo3 and COPI. The overexpressed GAP-dead R54K mutant appeared to associate more stably with the coat (Fig. 6A). This association was lost upon mutation of the tryptophan motif present at the C-terminus of Gcs1. Curiously, mutation of the ALPS motif strongly increased co-purification of Gcs1 with Glo3 (presumably via COPI). This stabilisation possibly reflects a decrease in Gcs1 dissociation from COPI due to a loss of curvature sensing via the ALPS motif or could indicate that the ALPS motif may mask the tryptophan motif in solution. We conclude that COPI can bind Glo3 and Gcs1 simultaneously and that this *in vitro* transient complex between Glo3/ArfGAP2/3, coatomer, and Gcs1/ArfGAP1 can be stabilized by manipulating Gcs1/ArfGAP1. This substantially strengthens our hypothesis that the two different ArfGAPs, akin to the two Arf GTPases, occupy

distinct molecular niches within the COPI coat (Fig. 1A and B; Dodonova et al. 2017; Suckling et al 2014).

The niche harboring β-Arf1 and plausibly also Gcs1/ArfGAP1 (Fig. 1A and 6A) plays an important role in the retrieval of HDEL/KDEL containing proteins. In this region of COPI, a recently discovered helix-b of δ-COP (Arakel et al., 2016; Dodonova et al., 2017) binds the switch and interswitch of β-Arf1, a region in Arf1 that is occluded by the N_O amphipathic helix in its inactive state (Dodonova et al., 2017). Given its ascribed role in cargo-sorting (Arakel et al., 2016), its association with Arf1 (Dodonova et al., 2017) and the recognised coupling of Arf1 GTP-hydrolysis to cargo sorting (Lanoix et al., 1999; Nickel et al., 1998), it is plausible that the helix translates GTP-hydrolysis in β-Arf1 to COPI.

Perturbation of genes encoding for machinery involved in retrograde trafficking results in the secretion of HDEL- (KDEL- in higher eukaryotes) bearing soluble and luminal ER residents such as chaperones (Aguilera-Romero et al., 2008; Belden and Barlowe, 2001). Secretion of HDEL containing proteins can occur either due to the inefficient retrieval of the HDEL receptor (Erd2) or the activation of the unfolded protein response (UPR) where the capacity of the HDEL-retrieval pathway is overwhelmed by the elevated expression of HDEL-bearing chaperones. Both situations are entwined and not mutually exclusive.

Deletion of Gcs1 leads to the secretion of HDEL-bearing Pdi1 (Fig. 6B and 6C) and the induction of UPR (Jonikas et al., 2009). Deletion of the δ-COP helix-b which contacts β-Arf1 also results in the secretion of Pdi1 (Fig. 6B and 6C). Expression of functional Gcs1, but not GAP-dead Gcs1 rescues the observed secretion phenotype in a Gcs1 deletion strain, implying that GAP-stimulated GTP hydrolysis regulates HDEL retrieval. The upstream role of this specific ArfGAP and

the downstream role of the δ-COP helix-b in the retrieval of the HDEL-bearing Pdi1 imply that δ-COP may relay the GTP-hydrolysis in β-Arf1 to COPI.

Deletion of Glo3 also leads to the secretion of HDEL-bearing Pdi1 (Fig. 6B-6E) and the induction of UPR (Jonikas et al., 2009). Expression of Glo3 rescues the observed phenotype in a Glo3 deletion strain (Fig. 6D & 6E). However, expression of the only two viable GAP-dead (R59K) mutants, the GRM deletion mutant and the S389, 398D phospho-mimetic mutant, did not rescue the secretion phenotype. In contrast, expression of the same mutants in combination with a functional GAP domain led to a complete rescue of the secretion phenotype (Fig. 6D & 6E). This suggests that the GRM domain of Glo3 does not play a crucial role in HDEL-cargo sorting while the GAP-domains of both Glo3 and Gcs1are central to efficient retrieval.

Discussion

Unlike the COPII vesicle coat, where GAP activity is exerted by the Sec23 coat subunit (Yoshihisa et al., 1993), COPI relies on at least two accessory GAPs to stimulate GTPase activity in Arf1. In COPII, assembly of the inner Sec23/24 coat complex with the outer cage (Sec13/31) further stimulates the GAP activity of Sec23 toward Sar1 (Antonny et al., 2001; Bi et al., 2007). Similar to COPII, COPI-associated ArfGAPs have higher activity when bound to both, Arf1 and COPI (Goldberg, 1999; Pevzner et al., 2012). COPI and both ArfGAPs bind Arf1 non-competitively unlike other GTPases, which bind GAPs or their effectors in a competitive manner (Chen et al., 2012; Clabecq et al., 2000; Puertollano et al., 2001). This mechanism would require that the COPI-associated ArfGAPs are subject

to regulation at multiple levels. ArfGAPs have also been implicated in cargo recognition and binding (Lee et al., 2005; Rein et al., 2002). Once bound, cargo regulates the activity of the ArfGAPs potentially contributing to yet another tier of regulation (Goldberg, 1999; Luo et al., 2009). It is therefore not surprising that the precise orchestration of GTP-hydrolysis in Arf1 has remained a perplexing question in the COPI vesicle cycle.

ArfGAP1 activity is enhanced with increasing membrane curvature. This feature has been attributed to an amphipathic helix (ALPS) in ArfGAP1/Gcs1, which is unstructured in solution (Bigay et al., 2005; Bigay et al., 2003). This helix senses lipid-packing defects, caused by the continual membrane curvature during vesicle formation, thereby determining the timing of catalytic activity in ArfGAP1. Like ArfGAP1, the activity of ArfGAP2 is enhanced in the presence of an intact coat (Goldberg, 1999; Luo et al., 2009; Pevzner et al., 2012; Szafer et al., 2001; Weimer et al., 2008). However, increasing membrane curvature does not enhance ArfGAP2 activity. The ArfGAP2 catalytic domain occupies a niche adjacent to γ-Arf1 that is formed only upon coat polymerisation, potentially providing one layer of regulation regarding its catalytic activity (Dodonova et al., 2017).

Owing to their overlapping functions, which may become apparent only under a strong selection pressure, both Gcs1 and Glo3 are non-essential. However, the combined deletion of both is lethal (Poon et al., 1999). Cell viability is not compromised upon the defective targeting of either Gcs1 and Glo3 to COPI. Deletion of the μHD (Arakel et al., 2016), mutation of the tryptophan-motif in Gcs1 (Suckling et al., 2014), deletion of the γ-appendage domain or mutation of its COPI binding site (Watson et al., 2004) or the mutation of the COPI binding region in Glo3 did not affect cell growth (Fig. 3B). However, using GAP-dead mutants *in vivo*, we now

establish that cell viability is compromised when a GAP-dead Glo3 occupies its niche. This is in marked contrast to a GAP-dead Gcs1, where cell viability remains unaffected.

Inhibition of GTP-hydrolysis in γ-Arf1 appears to abrogate the execution of a function essential for cell survival. Our findings reveal that cell viability is restored by impeding the function of the Glo3 regulatory motif (GRM) either by its deletion or through its phosphorylation (phosphomimetic substitution), suggesting that GTP-hydrolysis in γ-Arf culminates in the execution of a critical function through the GRM domain (Fig. 7A). Conceivably, GTP-hydrolysis in γ-Arf1 executes this critical role through a conformational change, relayed either directly or indirectly to the GRM domain (Fig. 5D).

Inhibition of GTP hydrolysis by employing a GTP locked form of Arf1[Q71L] or the use of non-hydrolysable analogues prevents membrane release of COPI (Presley et al., 2002; Tanigawa et al., 1993). Vesicle uncoating is a prerequisite of fusion and for the recycling of all coat components and occurs as a direct consequence of GAP-driven GTP hydrolysis. Given the importance of vesicle uncoating, the recycling of coat components and the crucial nature of the GTP-hydrolysis in γ-Arf1, it is tempting to speculate that γ-Arf1, seated at the heart of a COPI triad (Dodonova et al., 2017), is primarily responsible for triggering coat disassembly.

We propose that at the centre of the triad (Fig. 7B), Glo3, which is tethered to the appendage domain of γ-COP, contacts other neighbouring Glo3 molecules or adjacent COPI heptamers of the triad via their GRM domain, effectively cross-linking individual coat molecules of the triad (Fig. 7C and 7E). GTP hydrolysis in γ-Arf1 and the subsequent conformational change in the GRM domain would disengage such a

lock, freeing individual coat molecules for disassociation (Fig. 7D). In a mutant lacking GAP activity, this feedback would be lost rendering individual coat molecules incapable of efficient disassembly from the triad and the membrane. Deletion of the GRM or electrostatic repulsion between its phosphorylated side chains possibly prevents the formation of such a lock alleviating its adverse impact in the GAP-dead mutant. Moreover, or alternatively, phosphorylation may accelerate the unlocking of the COPI triad. In addition to the γ-appendage sandwich subdomain contacting β'-COP (Dodonova et al., 2017), a mechanism in which the GRM domains interact homotypically (Fig. 7C) or crosslink individual COPI heptamers in the triad (Fig. 7E) may help further stabilise the COPI triad.

Such a model would help clarify why the over-expression of Glo3, with an intact GRM domain, mitigates the temperature-sensitivity of mutants harbouring mutations in the appendage domain of β-COP or in Arf1 (De Regis et al., 2008; Yahara et al., 2006). Mutations in the β-COP appendage, which serves as the main link between the cage-like (outer) and adaptor-like (inner) subcomplexes of the coat, (Dodonova et al., 2017), potentially destabilise the structure of the COPI coat and undermine its stability on membranes. The over-expression of Glo3 possibly ensures that its availability is not rate limiting and facilitates adequate buttressing of the triad (Fig. 7).

Phosphorylation and dephosphorylation of the GRM domain of Glo3 influences the dissociation of Arf1 from Golgi membranes (Fig 4E). By influencing the dwell-time of COPI on membranes, this model would also help explain both the 'productive' and 'discard/futile states' in the formation of COPI vesicles (Goldberg, 2000; Nie and Randazzo, 2006; Springer et al., 1999). The phospho-regulation of the possible stabilizing effect by Snf1 may additionally serve as a kinetic timer that delineates productive from unproductive cycles or accelerates unlocking of the triad.

S432 in human ArfGAP2 and S431 in mice, corresponding to S389 in Glo3, has been detected to be phosphorylated in nearly 50 high-throughput studies (www.phosphosite.org) suggesting that this phosphorylation of the Glo3 motif by AMPK is evolutionarily conserved and physiologically relevant. Indeed, our finding fits other observations that suggest a regulation of retrograde traffic in the Golgi by AMPK (Miyamoto et al., 2008).

Our model also explains why the deletion of Glo3 leads to a secretion of HDEL-bearing Pdi1. Curtailing the dwell time of COPI on the membrane by the deletion of Glo3 possibly affects the efficient sorting of cargo. In a similar manner, plasma membrane localised Snc1, whose recycling involves the first propeller domain of β'-COP (Xu et al., 2017), is mislocalised upon deletion of either Glo3 or Gcs1 (Kawada et al., 2015; Robinson et al., 2006). Although culminating in phenotypically similar outcomes the underlying mechanism by which Gcs1 or Glo3 deletion causes HDEL-protein secretion is likely distinct.

Why have the two ArfGAPs evolved seemingly different affinities for the COPI coat? It is not known if ArfGAP2/Glo3 is associated with coatomer in the cytosol and recruited to membranes *en bloc* or if the detected stable association of COPI and Glo3 (Fig. 1) represents COPI triads undergoing dissociation in the cytosol.

β-Arf, which occupies a region of the coated vesicle where the membrane is more exposed (Dodonova et al., 2017), is conceivably more actively involved in cargo-sorting and release (Fig. 6). The δ-COP helix-b potentially relays the GTPase activity of β-Arf1 to COPI by functionally translating this signal into a cargo-binding/release directive. The region adjoining the longin domain of ζ-COP is also predicted to form an α-helix equivalent to the δ-COP helix-b (Alisaraie and Rouiller, 2012). It is unknown if such a helix does exist or if GTP-hydrolysis in γ-Arf1 is

relayed to the coat. The pivotal role of GTP-hydrolysis in γ-Arf1 raises the possibility that this may have contributed to the evolutionary selective pressure underlying the gene duplication event in γ-COP, ζ-COP and ArfGAP2/3. The alternative isoforms of γ-COP, ζ-COP and ArfGAP2/3 (Kliouchnikov et al., 2008; Moelleken et al., 2007) suggest additional plasticity of GTP-hydrolysis in mammalian γ-Arf1, which may be modulated depending on the associated COPI isoform and ArfGAP2/3.

Although we can still only speculate about the precise mechanism by which COPI and ArfGAPs communicate, our data culminates in a model that reconciles the convoluted reports regarding the roles of Gcs1/ArfGAP1 and Glo3/ArfGAP2/3 in COPI vesicle biogenesis and uncoating.

Materials & Methods:

Yeast strains and plasmids.

The CloNAT cassette was amplified from the pAG25 vector. The cassette was inserted in the yeast genome by homologous recombination into the respective strains, deleting *GLO3* or *GCS1*. The knockout strains were verified by PCR from genomic DNA, using ORF-specific primers and antibodies against Glo3 and Gcs1. Yeast strains and plasmids employed in this study have been listed in Appendix Tables S1 and S2 respectively.

Affinity chromatography

Yeast cells were grown to mid-logarithmic phase and harvested. The cell pellet was flash-frozen in liquid nitrogen, crushed by hand and resuspended in lysis buffer 25

mM Tris pH 7.4, 50 mM KCl, 10 mM $MgCl_2$, 5% glycerol, 1% Triton X-100. Detergent was not added to the lysis buffer for the preparation of cytosolic extracts. After thawing, the samples were incubated on ice for 15 minutes. The extracts were centrifuged and the supernatant incubated with Miltenyi µMACS GFP micro-beads for 30 minutes at 4°C. The affinity matrix and bound complexes were separated using Miltenyi µMACS isolation columns. The matrix was washed four times with lysis buffer and eluted with SDS-sample buffer containing 100 mM DTT. The samples were either analysed by SDS-PAGE and Western blotting or by LC-MS/MS analysis.

Spotting assays

To control the expression, genes were placed downstream of the repressible *Met25* promoter. Yeast cells were transformed with the indicated plasmids and grown on synthetic complete media lacking leucine (auxotrophic marker) and containing excess methionine (800 µM) to repress gene expression. Transformed cells were normalised (OD_{600}) and spotted on low methionine containing synthetic complete media to induce gene expression. Cells were grown at 30°C for 3 days prior to analysis.

***In vitro* reconstitution of the COPI-Glo3 complex**

Rosetta (DE3) and BL21 (pREP4) *Escherichia coli* strains containing the MBP fusion constructs were induced by the addition of 0.2 mM IPTG at OD_{600} 0.8 for 3 h at 30°C. Cells were harvested and sonicated in lysis buffer [50 mM NaH_2PO_4, 300 mM NaCl, 15 mM imidazole, pH 8.0]. Lysates were cleared first at 5,000 × g for 5 min and subsequently at 100,000 × g for 30 min. The MBP fusion- proteins/baits were

purified by incubating lysates with Ni-IDA resin. The affinity matrix was washed five times with lysis buffer and eluted with elution buffer [50 mM NaH_2PO_4, 300 mM NaCl, 250 mM imidazole, pH 8.0]. The baits were dialyzed overnight in dialysis buffer (200 mM NaCl, 20 mM HEPES, pH 7.4, and 1 mM DTT) before use in *in vitro* reconstitution assays.

The TAP purification of COPI was performed as described in (Arakel et al., 2016). TAP-immobilised COPI was incubated with a molar excess of MBP-Glo3 (ΔAmpH) for 20 minutes at 4°C. The affinity matrix was washed three times with lysis buffer and once with TEV cleavage buffer (10 mM Tris-HCl, pH 8.0, 150 mM NaCl, 0.1% Triton X-100, 0.5 mM EDTA, and 1 mM DTT). The COPI-Glo3 complex was eluted by TEV cleavage for 1 h at 16°C. The eluates were incubated with amylose resin to deplete MBP.

Fluorescence recovery after photobleaching, data processing and analysis

Cells were grown in YPD media overnight, diluted and grown for 4-6 hr to mid-log phase in YPD or selective HC media supplemented with adenine. Glucose starvation was carried out for 2 hours prior FRAP measurement. Cells were washed and mounted in HC complete or selective media onto 1.6% agarose pad either with or without glucose. FRAP measurements were performed using Leica SP5-II-Matrix confocal microscope equipped with an oil immersion objective HCX Plan-Apochromat 63✕ NA 1.40-0.6 oil, Lbd Blue CS (± glucose experiment, Fig. 4D) or Leica TCS SP8 confocal microscope equipped with an oil immersion objective HC Plan-Apochromat 63x NA 1.4 oil, CS2 (Glo3 phosphomutants experiment, Fig. 4E) at 27°C. Data acquisition was performed in 512x512–pixel format with pinhole 2.62 Airy, at speed 1,000 Hz in bidirectional mode and 8-bits resolution. Bleaching (0.3 s)

was performed with a circular spot 1.0 μm in diameter using the 488 nm Ar line at 100% laser power. Fluorescence recovery was monitored at low laser intensity (2–5%) at 0.26 s intervals until reaching the plateau of recovery, in total for 43 seconds after bleach. 25-30 separate FRAP measurements were performed for each sample. All FRAP curves were double normalized to whole cell fluorescence loss during acquisition and background. Curve fitting was performed in GraphPad Prism software using the one-phase association fit assuming the protein turnover at the cis-Golgi to be an elementary association/dissociation process. All individual curves were fitted at once to obtain mean and 95% confidence interval of the desired parameters, rate constant k_{off} and the mobile fraction F_m.

Secretion assay

Secretions assays were performed as described in (Arakel et al., 2016)

Statistics

All experiments were reproduced no less than 3 times. The data was plotted as mean ± s.e.m. Statistical significance (P<0.05) was assessed by a two-tailed t-test.

Detection of Glo3 phosphorylation

Yeast strains expressing either Glo3-FLAG or variants thereof were grown to early-to-mid logarithmic phase in HC-Leu medium. Fifty OD_{600} per strain were harvested and resuspended in 500 μl of lysis buffer (25 mM Tris-HCL pH7.5, 250 mM KCl, 100 mM glycine, 1 mM β-mercaptoethanol, 1 μM $ZnCl_2$, 0.1% TritonX 100, 0.1 mM PMSF, protease inhibitor cocktail (Roche)). An equal volume of glass beads was added and the cells were lysed using Fast-Prep (MP Biomedical; 4x 15 sec at 6.5,

with 5' intervals on ice. After lysis, phosphatase inhibitors (10x: 100 mM NaF, 100 mM NaN$_3$, 100 mM pNPP, 100mM NaPPi, 100 mM β-glycerophosphate) were added when needed. Unbroken cells and debris were removed by centrifugation for 2 min at 3,000 rpm and 4°C. The supernatant was incubated with 20 µl of M2 anti-FLAG beads (Sigma) per 3 mg of cell lysate for 2 hrs at 4°C. The beads were washed 3x in lysis buffer and 3x in wash buffer (25 mM Tris-HCl pH 8.0, 150 mM NaCl). The samples were analysed either by gel electrophoresis or mass spectrometry. When indicated, samples were treated with alkaline phosphatase for 1 hr at 37°C prior to further analysis.

For gel analysis, samples were separated on 10% Phos-tag gels (Nard Technologies), transferred onto nitrocellulose and decorated with either a homemade or a commercially available anti-FLAG antibody and developed using a secondary anti-mouse-HRP antibody (Pierce 1:10,000) and ECL (GE Healthcare). For LC/MS/MS analysis, the beads were resuspended in 50 µl wash buffer. Protein digestion was started by adding 0.25 µg of ELC (Wako chemicals) and incubated for 2 hrs at 37°C. Digestion was continued with another 0.25 µg of ELC and 2 hr-incubation at 37°C. This was followed by a 2-step digestion with trypsin (1x 0.25 µg, 2 hr, 37°C and 1x 0.25 µg, over night at 37°C). The peptides were collected by centrifuging the beads for 2 min at 2,000 rpm and the supernatant was acidified by the addition of 1/20 vol. of 10% trifluoro-acetic acid. The samples were desalted using Microspin Vydac C18 silica columns according to the manufacturer's recommendation (The Nest group, Southborough, MA). The desalted peptides were dried and phosphopeptides were enriched with TiO$_2$ according to [1]. The phosphopeptide pool was desalted as above and analyzed on an Orbitrap Elite instrument as described in [2].

Glo3 purification for kinase assay

Glo3, Glo3(214-493) [Glo3-H], and Glo3(214-493 S->A)[Glo3-H13] were expressed in a 1 l culture of *E. coli* BL21* as N-terminal His-SUMO fusion proteins. Bacterial pellets were lysed in 30 ml of 20 mM Tris-HCl pH 7.8, 200 mM KCl, 1% Tween 20 in the presence of 1 mg/ml lysozyme and protease inhibitor through sonication. The lysate was spun for 30' at 24,000 g and 4°C. The supernatant was incubated with 0.4 g Protino Ni resin (Machery & Nagel) for 1hr at 4°C rotating end to end. The beads were washed 4x with 20 mM Tris-HCl pH 7.8, 200 mM KCl, 0.1% Tween 20, 2x with 20 mM Tris-HCl pH 7.8, 1 M KCl, 0.1% Tween 20 and again once with 20 mM Tris-HCl pH 7.8, 200 mM KCl, 0.1% Tween 20. Proteins were eluted with 250 mM imidazole in 20 mM Tris-HCl pH 7.8, 200 mM KCl, protein containing fractions were pooled and dialyzed 3x against PBS 5% glycerol. The proteins were snap frozen in liquid N_2 and stored at -80°C.

Snf1 kinase assay

The Snf1 kinase assay is based on [3,4]. Cells expressing Snf1-HA or the kinase mutant Snf1-K84R-HA or ∆*snf1* were collected by filtration, resuspended in SC complete (0.5% glucose) and incubated under shaking at 30°C for 20 min, collected again by filtration and stored at -80°C. After cell lysis through vortexing in 50 mM Tris-HCl pH 7.5, 50 mM NaF, 5 mM Na^+ pyrophosphate, 1 mM EDTA, 0.5% TX100, 10% (vol/vol) glycerol and protease inhibitor cocktail (Pierce), the lysate was spun 10 min, 13,000 g, 4°C, the supernatant transferred to a fresh microfuge tube and spun 5 min, 13,000 g, 4°C. The supernatant was incubated with 40 µl 50% slurry of anti-HA beads (Thermo Scientific) for 2 hrs at 4°C under end to end rotation. The beads

were washed 3x with 50 mM Tris-HCl pH 7.5, 150 mM NaCl, 50 mM NaF, 1 mM EDTA, 1 mM DTT and protease inhibitors (Pierce) and 2x in 1x kinase buffer (20 mM HEPES pH 7.5, 100 mM NaCl, 0.5 mM EDTA, 5 mM MgAc$_2$, 0.5 mM DTT. The IP efficiency was evaluated by immunoblot. Snf1-HA or the kinase mutant were incubated with 6 µg of Glo3 or Glo3 variants in 1x kinase buffer and the presence of 100 µCi/ml ^{32}P-ATP (SRP-301) and 1 mM ATP in a total reaction volume of 30 µl for 60 min at 30°C. 13 µl of the reaction was separated on a 4-15% SDS-PAGE gradient gel. The gel was stained with Coomassie blue and a picture was taken of the gel before drying it on a filter paper for autoradiography.

Acknowledgements

Author contributions

ECA and BS conceptualized and designed the structure-based functional dissection of COPI and the ArfGAPs. AS conceptualized and designed the study regarding the regulation of Glo3 by phosphorylation. AS, AFE, MH and EMR identified the sites of phosphorylation in Glo3 and Snf1 as the relevant kinase (Fig. 4 and S3). MH designed, performed, analyzed FRAP experiments. ECA performed the remaining experiments. ECA drafted the manuscript and developed the model. ECA, BS, and AS discussed and revised the manuscript. BS and AS secured funding.

References

Aguilera-Romero, A., Kaminska, J., Spang, A., Riezman, H. and Muñiz, M. (2008). The yeast p24 complex is required for the formation of COPI retrograde transport vesicles from the Golgi apparatus. *J Cell Biol* **180**, 713–720.

Alisaraie, L. and Rouiller, I. (2012). Full-length structural model of RET3 and SEC21 in COPI: identification of binding sites on the appendage for accessory protein recruitment motifs. *J Mol Model* **18**, 3199–3212.

Aniento, F., Gu, F., Parton, R. G. and Gruenberg, J. (1996). An endosomal beta COP is involved in the pH-dependent formation of transport vesicles destined for late endosomes. *J Cell Biol* **133**, 29–41.

Antonny, B., Beraud-Dufour, S., Chardin, P. and Chabre, M. (1997). N-terminal hydrophobic residues of the G-protein ADP-ribosylation factor-1 insert into membrane phospholipids upon GDP to GTP exchange. *Biochemistry* **36**, 4675–4684.

Antonny, B., Madden, D., Hamamoto, S., Orci, L. and Schekman, R. (2001). Dynamics of the COPII coat with GTP and stable analogues. *Nat Cell Biol* **3**, 531–537.

Arakel, E. C., Richter, K. P., Clancy, A. and Schwappach, B. (2016). δ-COP contains a helix C-terminal to its longin domain key to COPI dynamics and function. *Proc Natl Acad Sci U S A*.

Beck, R., Rawet, M., Ravet, M., Wieland, F. T. and Cassel, D. (2009). The COPI system: molecular mechanisms and function. *FEBS Lett* **583**, 2701–2709.

Belden, W. J. and Barlowe, C. (2001). Deletion of yeast p24 genes activates the unfolded protein response. *Mol. Biol. Cell* **12**, 957–969.

Beller, M., Sztalryd, C., Southall, N., Bell, M., Jäckle, H., Auld, D. S. and Oliver, B. (2008). COPI complex is a regulator of lipid homeostasis. *PLoS Biol.* **6**, e292.

Bi, X., Mancias, J. D. and Goldberg, J. (2007). Insights into COPII coat nucleation from the structure of Sec23.Sar1 complexed with the active fragment of Sec31. *Dev. Cell* **13**, 635–645.

Bigay, J., Casella, J.-F., Drin, G., Mesmin, B. and Antonny, B. (2005). ArfGAP1 responds to membrane curvature through the folding of a lipid packing sensor motif. *EMBO J* **24**, 2244–2253.

Bigay, J., Gounon, P., Robineau, S. and Antonny, B. (2003). Lipid packing sensed by ArfGAP1 couples COPI coat disassembly to membrane bilayer curvature. *Nature* **426**, 563–566.

Blom, N., Gammeltoft, S. and Brunak, S. (1999). Sequence and structure-based prediction of eukaryotic protein phosphorylation sites. *J. Mol. Biol.*

Braun, K. A., Vaga, S., Dombek, K. M., Fang, F., Palmisano, S., Aebersold, R. and Young, E. T. (2014). Phosphoproteomic analysis identifies proteins involved in transcription-coupled mRNA decay as targets of Snf1 signaling. *Sci Signal* **7**, ra64–ra64.

Bykov, Y. S., Schaffer, M., Dodonova, S. O., Albert, S., Plitzko, J. M., Baumeister, W., Engel, B. D. and Briggs, J. A. (2017). The structure of the COPI coat determined within the cell. *Elife* **6**, e32493.

Chen, K.-Y., Tsai, P.-C., Liu, Y.-W. and Lee, F.-J. S. (2012). Competition between the golgin Imh1p and the GAP Gcs1p stabilizes activated Arl1p at the late-Golgi. **125**, 4586–4596.

Clabecq, A., Henry, J. P. and Darchen, F. (2000). Biochemical characterization of Rab3-GTPase-activating protein reveals a mechanism similar to that of Ras-GAP. *J. Biol. Chem.* **275**, 31786–31791.

Cosson, P., Lefkir, Y., Démollière, C. and Letourneur, F. (1998). New COP1-binding motifs involved in ER retrieval. *EMBO J* **17**, 6863–6870.

De Regis, C. J., Rahl, P. B., Hoffman, G. R., Cerione, R. A. and Collins, R. N. (2008). Mutational analysis of betaCOPI (Sec26p) identifies an appendage domain critical for function. *BMC Cell Biol* **9**, 3.

Dodonova, S. O., Aderhold, P., Kopp, J., Ganeva, I., Röhling, S., Hagen, W. J. H., Sinning, I., Wieland, F. and Briggs, J. A. G. (2017). 9Å structure of the COPI coat reveals that the Arf1 GTPase occupies two contrasting molecular environments. *Elife* **6**, e26691.

Dodonova, S. O., Diestelkoetter-Bachert, P., Appen, von, A., Hagen, W. J. H., Beck, R., Beck, M., Wieland, F. and Briggs, J. A. G. (2015). A structure of the COPI coat and the role of coat proteins in membrane vesicle assembly. *Science* **349**, 195–198.

Frigerio, G., Grimsey, N., Dale, M., Majoul, I. and Duden, R. (2007). Two human ARFGAPs associated with COP-I-coated vesicles. *Traffic* **8**, 1644–1655.

Goldberg, J. (1999). Structural and functional analysis of the ARF1-ARFGAP complex reveals a role for coatamer in GTP hydrolysis. *Cell* **96**, 893–902.

Goldberg, J. (2000). Decoding of sorting signals by coatamer through a GTPase switch in the COPI coat complex. *Cell* **100**, 671–679.

Hara-Kuge, S., Kuge, O., Orci, L., Amherdt, M., Ravazzola, M., Wieland, F. T. and Rothman, J. E. (1994). En bloc incorporation of coatamer subunits during the assembly of COP-coated vesicles. *J Cell Biol* **124**, 883–892.

Hardie, D. G., Carling, D. and Carlson, M. (1998). The AMP-activated/SNF1 protein kinase subfamily: metabolic sensors of the eukaryotic cell? *Annu. Rev. Biochem.* **67**, 821–855.

Huranova, M., Muruganandam, G., Weiss, M. and Spang, A. (2016). Dynamic

assembly of the exomer secretory vesicle cargo adaptor subunits. *EMBO Rep.* **17**, 202–219.

Jonikas, M. C., Collins, S. R., Denic, V., Oh, E., Quan, E. M., Schmid, V., Weibezahn, J., Schwappach, B., Walter, P., Weissman, J. S., et al. (2009). Comprehensive characterization of genes required for protein folding in the endoplasmic reticulum. *Science* **323**, 1693–1697.

Kahn, R. A. and Gilman, A. G. (1986). The protein cofactor necessary for ADP-ribosylation of Gs by cholera toxin is itself a GTP binding protein. *J. Biol. Chem.* **261**, 7906–7911.

Kawada, D., Kobayashi, H., Tomita, T., Nakata, E., Nagano, M., Siekhaus, D. E., Toshima, J. Y. and Toshima, J. (2015). The yeast Arf-GAP Glo3p is required for the endocytic recycling of cell surface proteins. *Biochim. Biophys. Acta* **1853**, 144–156.

Kliouchnikov, L., Bigay, J., Mesmin, B., Parnis, A., Rawet, M., Goldfeder, N., Antonny, B. and Cassel, D. (2008). Discrete Determinants in ArfGAP2/3 Conferring Golgi Localization and Regulation by the COPI Coat. *Mol. Biol. Cell* **20**, 859–869.

Lanoix, J., Ouwendijk, J., Lin, C. C., Stark, A., Love, H. D., Ostermann, J. and Nilsson, T. (1999). GTP hydrolysis by arf-1 mediates sorting and concentration of Golgi resident enzymes into functional COP I vesicles. *EMBO J* **18**, 4935–4948.

Lee, S. Y., Yang, J.-S., Hong, W., Premont, R. T. and Hsu, V. W. (2005). ARFGAP1 plays a central role in coupling COPI cargo sorting with vesicle formation. *J Cell Biol* **168**, 281–290.

Lewis, S. M., Poon, P. P., Singer, R. A., Johnston, G. C. and Spang, A. (2004). The ArfGAP Glo3 is required for the generation of COPI vesicles. *Mol. Biol. Cell* **15**, 4064–4072.

Luo, R., Ha, V. L., Hayashi, R. and Randazzo, P. A. (2009). Arf GAP2 is positively regulated by coatomer and cargo. *Cell. Signal.* **21**, 1169–1179.

Miyamoto, T., Oshiro, N., Yoshino, K.-I., Nakashima, A., Eguchi, S., Takahashi, M., Ono, Y., Kikkawa, U. and Yonezawa, K. (2008). AMP-activated protein kinase phosphorylates Golgi-specific brefeldin A resistance factor 1 at Thr1337 to induce disassembly of Golgi apparatus. *J. Biol. Chem.* **283**, 4430–4438.

Moelleken, J., Malsam, J., Betts, M. J., Movafeghi, A., Reckmann, I., Meissner, I., Hellwig, A., Russell, R. B., Söllner, T., Brügger, B., et al. (2007). Differential localization of coatomer complex isoforms within the Golgi apparatus. *Proc Natl Acad Sci U S A* **104**, 4425–4430.

Nickel, W., Malsam, J., Gorgas, K., Ravazzola, M., Jenne, N., Helms, J. B. and Wieland, F. T. (1998). Uptake by COPI-coated vesicles of both anterograde and retrograde cargo is inhibited by GTPgammaS in vitro. **111 (Pt 20)**, 3081–3090.

Nie, Z. and Randazzo, P. A. (2006). Arf GAPs and membrane traffic. **119**, 1203–1211.

Pellett, P. A., Dietrich, F., Bewersdorf, J., Rothman, J. E. and Lavieu, G. (2013). Inter-Golgi transport mediated by COPI-containing vesicles carrying small cargoes. *Elife* **2**, e01296.

Pevzner, I., Strating, J., Lifshitz, L., Parnis, A., Glaser, F., Herrmann, A., Brügger, B., Wieland, F. and Cassel, D. (2012). Distinct role of subcomplexes of the COPI coat in the regulation of ArfGAP2 activity. *Traffic* **13**, 849–856.

Poon, P. P., Cassel, D., Spang, A., Rotman, M., Pick, E., Singer, R. A. and Johnston, G. C. (1999). Retrograde transport from the yeast Golgi is mediated by two ARF GAP proteins with overlapping function. *EMBO J* **18**, 555–564.

Poon, P. P., Nothwehr, S. F., Singer, R. A. and Johnston, G. C. (2001). The Gcs1 and Age2 ArfGAP proteins provide overlapping essential function for transport from the yeast trans-Golgi network. *J Cell Biol* **155**, 1239–1250.

Presley, J. F., Ward, T. H., Pfeifer, A. C., Siggia, E. D., Phair, R. D. and Lippincott-Schwartz, J. (2002). Dissection of COPI and Arf1 dynamics in vivo and role in Golgi membrane transport. *Nature* **417**, 187–193.

Puertollano, R., Randazzo, P. A., Presley, J. F., Hartnell, L. M. and Bonifacino, J. S. (2001). The GGAs promote ARF-dependent recruitment of clathrin to the TGN. *Cell* **105**, 93–102.

Randazzo, P. A. and Hirsch, D. S. (2004). Arf GAPs: multifunctional proteins that regulate membrane traffic and actin remodelling. *Cell. Signal.* **16**, 401–413.

Randazzo, P. A. and Kahn, R. A. (1994). GTP hydrolysis by ADP-ribosylation factor is dependent on both an ADP-ribosylation factor GTPase-activating protein and acid phospholipids. *J. Biol. Chem.* **269**, 10758–10763.

Rawet, M., Levi-Tal, S., Szafer-Glusman, E., Parnis, A. and Cassel, D. (2010). ArfGAP1 interacts with coat proteins through tryptophan-based motifs. *Biochemical and Biophysical Research Communications* **394**, 553–557.

Rein, U., Andag, U., Duden, R., Schmitt, H. D. and Spang, A. (2002). ARF-GAP-mediated interaction between the ER-Golgi v-SNAREs and the COPI coat. *J Cell Biol* **157**, 395–404.

Rhiel, M., Hessling, B., Gao, Q., Hellwig, A., Adolf, F. and Wieland, F. T. (2018). Core Proteome and Architecture of COPI Vesicles. *bioRxiv* 254052.

Robinson, M., Poon, P. P., Schindler, C., Murray, L. E., Kama, R., Gabriely, G., Singer, R. A., Spang, A., Johnston, G. C. and Gerst, J. E. (2006). The Gcs1 Arf-GAP mediates Snc1,2 v-SNARE retrieval to the Golgi in yeast. *Mol. Biol. Cell* **17**, 1845–1858.

Schindler, C. and Spang, A. (2007). Interaction of SNAREs with ArfGAPs Precedes Recruitment of Sec18p/NSF. *Mol. Biol. Cell* **18**, 2852–2863.

Schindler, C., Rodriguez, F., Poon, P. P., Singer, R. A., Johnston, G. C. and Spang, A. (2009). The GAP Domain and the SNARE, Coatomer and Cargo Interaction Region of the ArfGAP2/3 Glo3 are Sufficient for Glo3 Function. *Traffic* **10**, 1362–1375.

Shibuya, A., Margulis, N., Christiano, R., Walther, T. C. and Barlowe, C. (2015). The Erv41-Erv46 complex serves as a retrograde receptor to retrieve escaped ER proteins. *The Journal of Cell Biology* **208**, 197–209.

Spang, A. and Schekman, R. (1998). Reconstitution of retrograde transport from the Golgi to the ER in vitro. *J Cell Biol* **143**, 589–599.

Spang, A., Shiba, Y. and Randazzo, P. A. (2010). Arf GAPs: gatekeepers of vesicle generation. *FEBS Lett* **584**, 2646–2651.

Springer, S., Spang, A. and Schekman, R. (1999). A Primer on Vesicle Budding. *Cell* **97**, 145–148.

Suckling, R. J., Poon, P. P., Travis, S. M., Majoul, I. V., Hughson, F. M., Evans, P. R., Duden, R. and Owen, D. J. (2014). The structural basis for the binding of tryptophan-based motifs by δ-COP.

Szafer, E., Rotman, M. and Cassel, D. (2001). Regulation of GTP hydrolysis on ADP-ribosylation factor-1 at the Golgi membrane. *J. Biol. Chem.* **276**, 47834–47839.

Tanigawa, G., Orci, L., Amherdt, M., Ravazzola, M., Helms, J. B. and Rothman, J. E. (1993). Hydrolysis of bound GTP by ARF protein triggers uncoating of Golgi-derived COP-coated vesicles. *J Cell Biol* **123**, 1365–1371.

Watson, P. J., Frigerio, G., Collins, B. M., Duden, R. and Owen, D. J. (2004). gamma-COP Appendage Domain - Structure and Function. *Traffic* **5**, 79–88.

Weill, U., Arakel, E. C., Goldmann, O., Golan, M., Chuartzman, S., Munro, S., Schwappach, B. and Schuldiner, M. (2018). Toolbox: Creating a systematic database of secretory pathway proteins uncovers new cargo for COPI. *Traffic* **19**, 370–379.

Weimer, C., Beck, R., Eckert, P., Reckmann, I., Moelleken, J., Brügger, B. and Wieland, F. (2008). Differential roles of ArfGAP1, ArfGAP2, and ArfGAP3 in COPI trafficking. *The Journal of Cell Biology* **183**, 725–735.

Xu, P., Baldridge, R. D., Chi, R. J., Burd, C. G. and Graham, T. R. (2013). Phosphatidylserine flipping enhances membrane curvature and negative charge required for vesicular transport. *The Journal of Cell Biology* **202**, 875–886.

Xu, P., Hankins, H. M., MacDonald, C., Erlinger, S. J., Frazier, M. N., Diab, N. S., Piper, R. C., Jackson, L. P., MacGurn, J. A. and Graham, T. R. (2017). COPI mediates recycling of an exocytic SNARE by recognition of a ubiquitin sorting signal. *Elife* **6**, e28342.

Yahara, N., Sato, K. and Nakano, A. (2006). The Arf1p GTPase-activating protein

Glo3p executes its regulatory function through a conserved repeat motif at its C-terminus. **119**, 2604–2612.

Yanagisawa, L. L., Marchena, J., Xie, Z., Li, X., Poon, P. P., Singer, R. A., Johnston, G. C., Randazzo, P. A. and Bankaitis, V. A. (2002). Activity of specific lipid-regulated ADP ribosylation factor-GTPase-activating proteins is required for Sec14p-dependent Golgi secretory function in yeast. *Mol. Biol. Cell* **13**, 2193–2206.

Yang, J.-S., Hsu, J.-W., Park, S.-Y., Li, J., Oldham, W. M., Beznoussenko, G. V., Mironov, A. A., Loscalzo, J. and Hsu, V. W. (2018). GAPDH inhibits intracellular pathways during starvation for cellular energy homeostasis. *Nature* **561**, 263–267.

Yang, J.-S., Lee, S. Y., Gao, M., Bourgoin, S., Randazzo, P. A., Premont, R. T. and Hsu, V. W. (2002). ARFGAP1 promotes the formation of COPI vesicles, suggesting function as a component of the coat. *J Cell Biol* **159**, 69–78.

Yoshihisa, T., Barlowe, C. and Schekman, R. (1993). Requirement for a GTPase-activating protein in vesicle budding from the endoplasmic reticulum. *Science* **259**, 1466–1468.

Yu, X., Breitman, M. and Goldberg, J. (2012). A Structure-Based Mechanism for Arf1-Dependent Recruitment of Coatomer to Membranes. *Cell* **148**, 530–542.

Figures
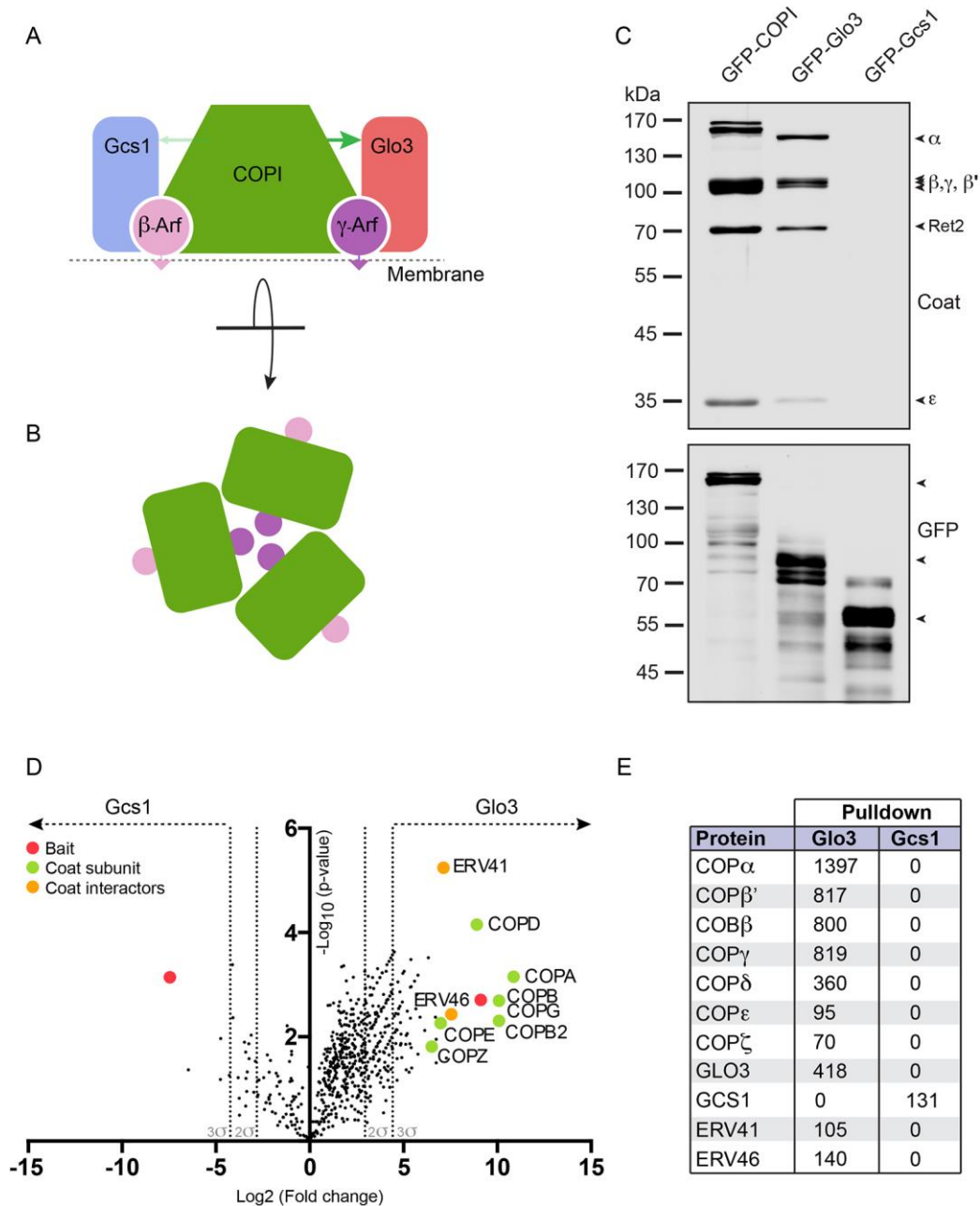
Fig. 1. COPI and Glo3 are stably associated

(A) Schematic illustration of the heptameric COPI coat in complex with two Arf1-

molecules (β-Arf1 and γ-Arf1) and the two ArfGAPs (Glo3 and Gcs1). The thickness

of the arrow indicates the differential affinity between COPI and the two ArfGAPs based on reports utilizing isolated domains (Suckling et al., 2014; Watson et al., 2004).

(B) Schematic illustration of the COPI triad, the symmetric basic unit of the coat. γ-Arf1 occupies the centre of a triad while β-Arf1 lies at the periphery where the membrane surface is more exposed.

(C) Eluates were analysed by Western blot detecting coat subunits (top) or the respective GFP fusion proteins (bottom) Affinity chromatography of GFP-tagged proteins isolated from the cytosol of the three indicated strains.

(D) Volcano plot analysis of proteins identified by mass spectrometry following the affinity chromatography of Glo3 and Gcs1 from detergent extracts of the indicated strains. The -log10 of the p-value indicating significance is plotted against the log2 of the enrichment. Coatomer subunits and the identified interaction partners, which are significantly enriched (>3σ), are coloured green and orange respectively.

(E) List and spectral counts of interaction partners identified by mass spectrometry following the affinity chromatography of Glo3 and Gcs1 from detergent extracts of the indicated strains. COPI and Glo3 appear to be in a stable complex. Compare Appendix Table S3 for a full list of co-purifying proteins.
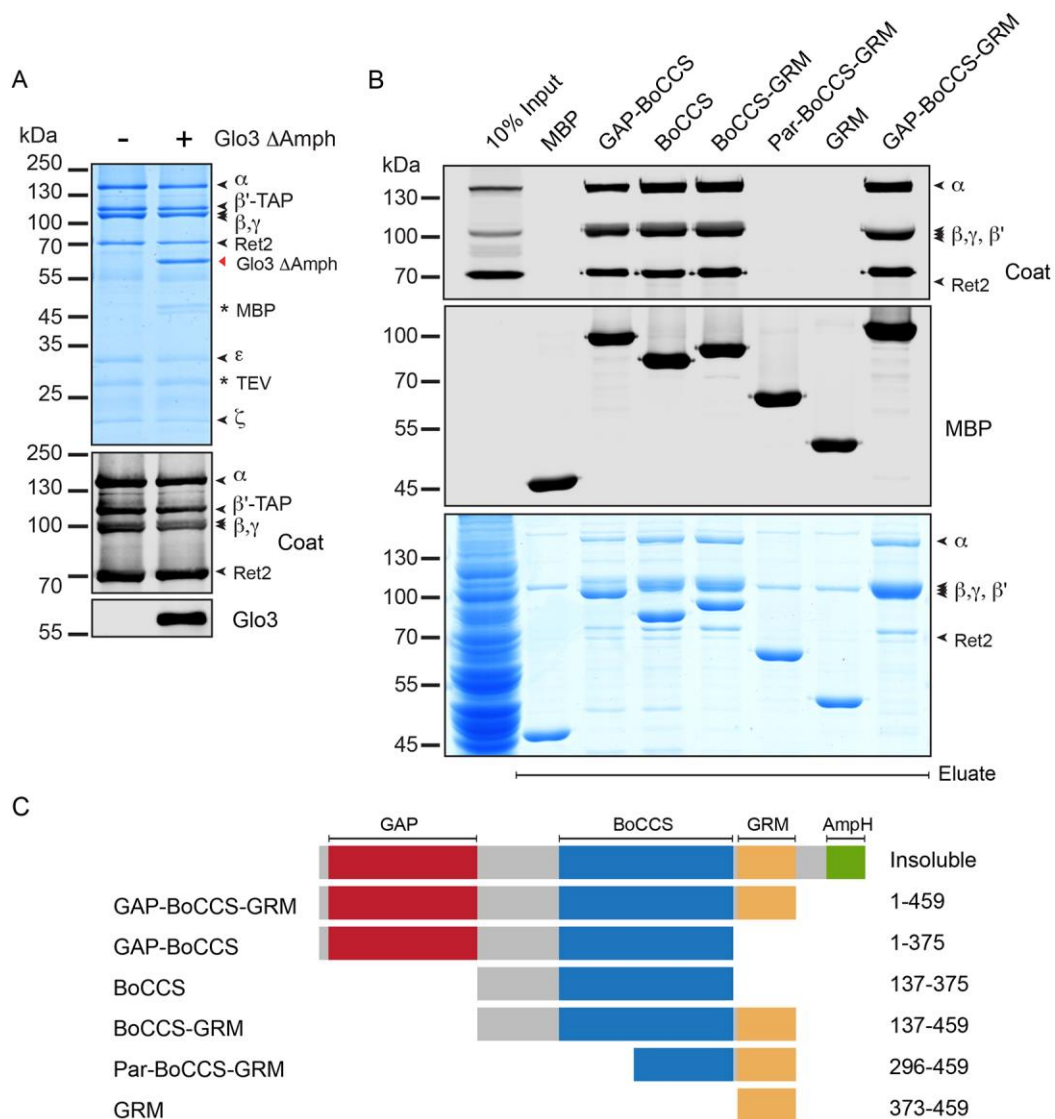
Fig. 2. Glo3 forms a stoichiometric complex with COPI *in vitro*

(A) *In vitro* reconstitution of a COPI-Glo3 complex using TAP-purified coatomer and recombinantly expressed and purified Glo3, lacking its distal amphipathic helix (459-493). Eluate obtained by tobacco-etch virus (TEV) protease elution of TAP-tagged β'-COP after incubation with Glo3 (1-459) was stained by Coomassie (Top) or analysed by Western blot (Bottom) using a coat antiserum detecting five of the seven subunits, or a Glo3 antibody.

(B) Binding of coatomer to MBP fusion proteins of Glo3 from yeast lysates. The bound fraction was eluted and analysed by SDS/PAGE. Western blots were detected

with a coat antiserum recognising five of the seven coatomer subunits.

(C) Schematic illustration of the MBP-tagged truncations of Glo3. GTPase activating domain (GAP), Binding of Coatomer, Cargo and SNARE domain (BoCCS), Glo3 motif (GRM), amphipathic helix (AmpH).
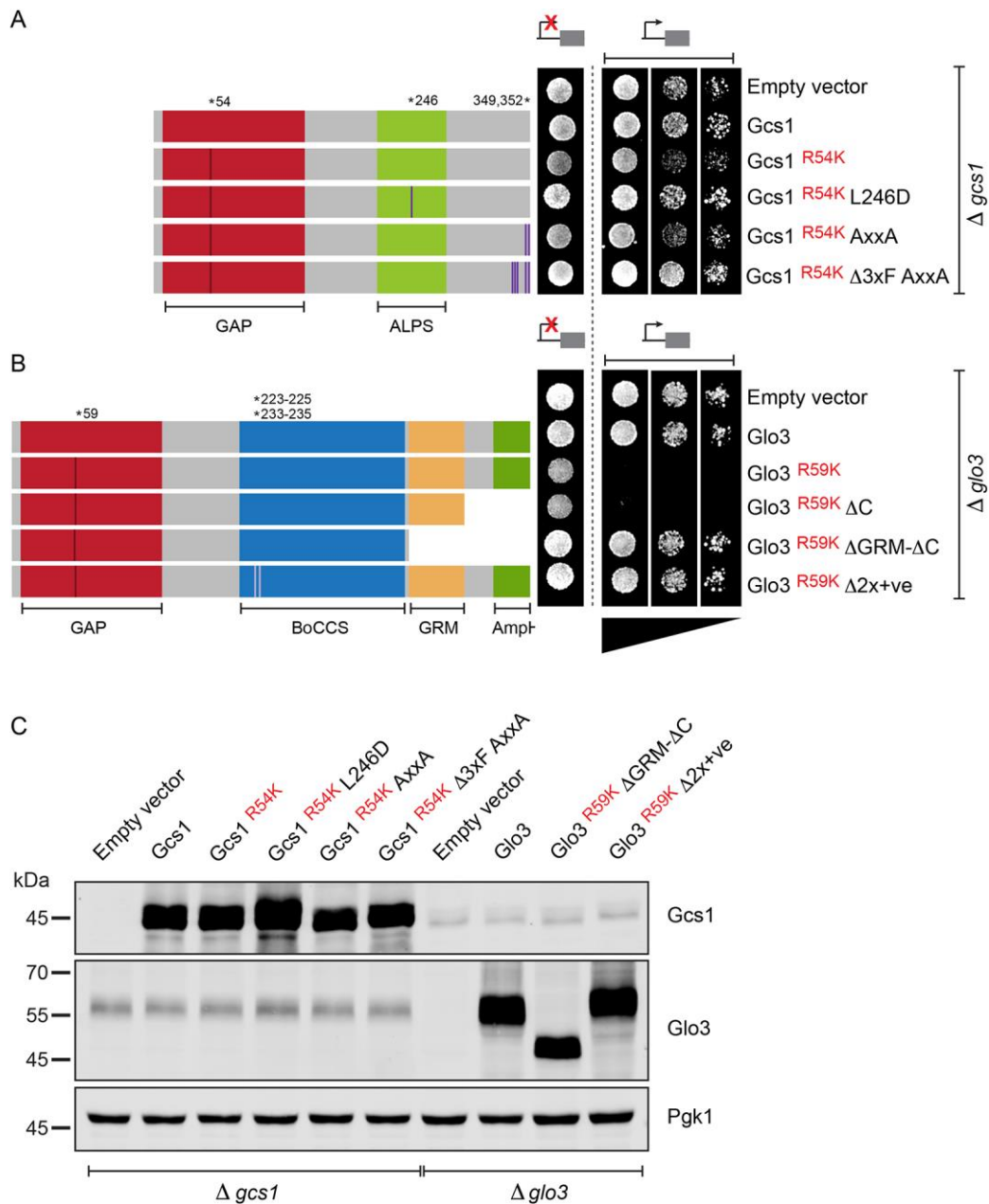
Fig. 3. Gcs1 and Glo3 regulate distinct cellular functions

(A) Growth assay. Growth of Δ*gcs1* strains harbouring the indicated constructs on synthetic dropout media was assayed in *MET25*-promoter repressing (high methionine; control indicated by scheme of a repressed promoter) and inducing (normal methionine; test indicated by scheme of an induced promoter) conditions. A GAP-dead mutant of Gcs1 (R54K) supports growth at 30°C. Gcs1 L246D – ALPS

mutant; Gcs1 AxxA – alanine substitution of C-terminal tryptophan-based COPI recognition signal; Gcs1 Δ3xF AxxA – alanine substitution of C-terminal tryptophan-based COPI recognition signal and three upstream phenylalanine's. GTPase activating domain (GAP), ArfGAP1 lipid packing sensor (ALPS).

(B) Growth assay. Growth of Δglo3 strains harbouring the indicated constructs on synthetic dropout media was assayed in MET25 promoter repressing (high methionine; Control) and inducing (normal methionine; Test) conditions. A GAP-dead mutant of Glo3 (R59K) does not support growth at 30°C indicating that GTP-hydrolysis stimulated by Glo3 in γ-Arf1 is essential. Glo3 ΔC – deletion of amphipathic helix; Glo3 ΔGRM-ΔC – combined deletion of the amphipathic helix and Glo3 motif; Glo3 Δ2x+ve – alanine substitution of COPI binding region. GTPase activating domain (GAP). Binding of Coatomer, Cargo and SNARE domain (BoCCS), Glo3 motif (GRM), amphipathic helix (AmpH).

(C) Expression analysis of proteins in the indicated strains grown in Met25 promoter inducing (normal methionine; Test) conditions.
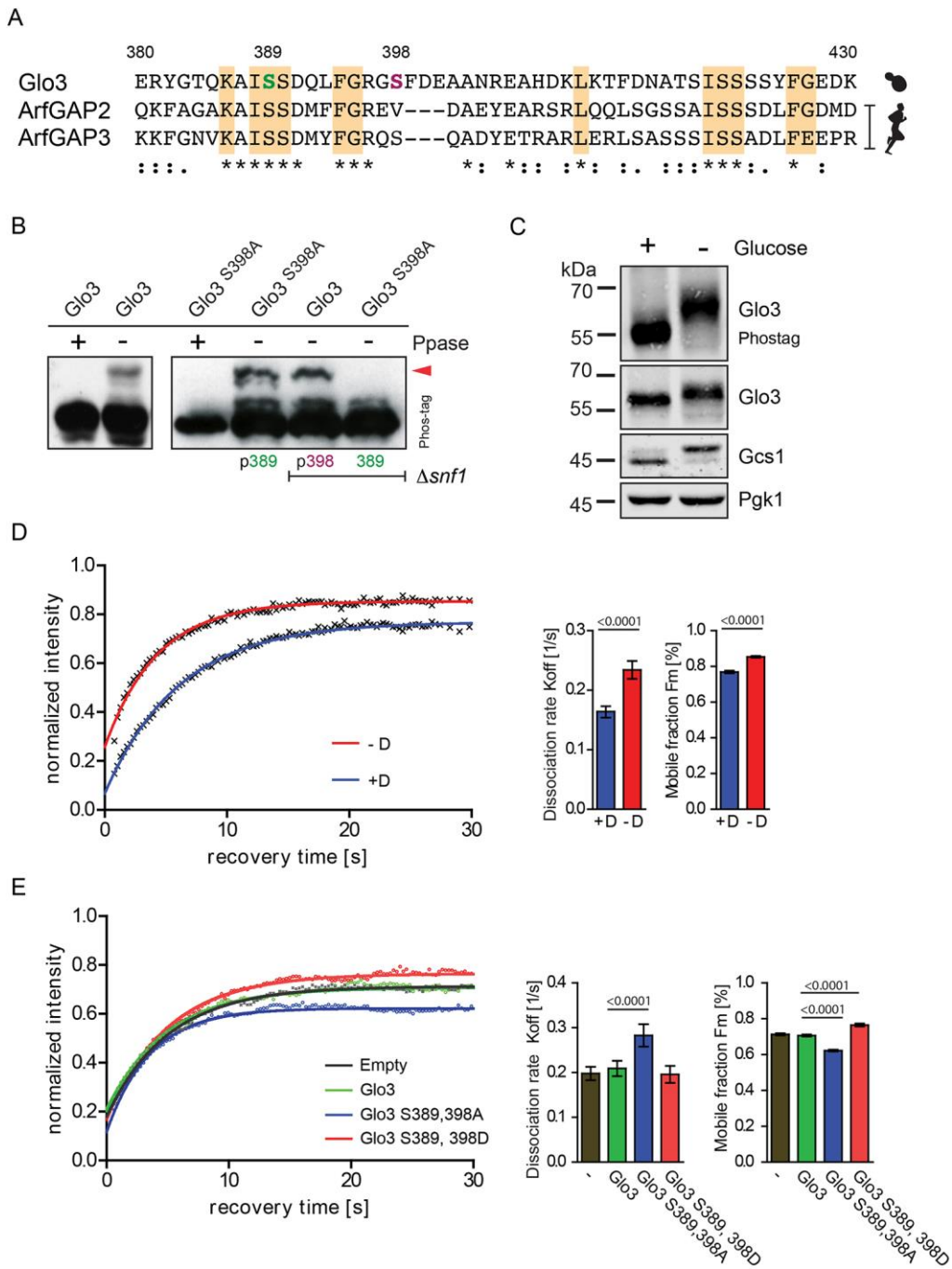
Fig. 4. Snf1 phosphorylates Glo3 serine 389

(A) Sequence alignment of the GRM domain of *S. cerevisiae* Glo3 and human

ArfGAP2 and ArfGAP3. Asterisks indicate fully conserved residues, colons and stops

indicate residues that are either strongly or weakly conserved. Regions of highest

conservation, when comparing other eukaryotes, are highlighted in orange.

(B) Δ*glo3* strains harbouring the indicated constructs under the control of a Tef1 promoter were analysed by Phos-tag PAGE. The electrophoretic mobility shift (arrowhead) indicates that S389 and S398 are phosphorylated in the presence and absence of the Snf1 kinase respectively. Treatment with λ-phosphatase (Ppase) resulted in dephosphorylation.

(C) Analysis of proteins by Phos-tag PAGE and SDS-PAGE following glucose starvation (± Glucose; ±D) for 3 hours in BY4741.

(D) Arf1-GFP fluorescence recovery after photobleach (FRAP) in the presence (+D) or absence (-D) of glucose. Cells were grown to mid-logarithmic phase and glucose starved for a period of 2 hours prior to FRAP measurement. The plot, reflecting the recovery of Arf1-GFP at Golgi membranes (Vrg4-mCherry), represents the mean FRAP curves with the fits.

(E) Arf1-GFP fluorescence recovery after photobleaching (FRAP) analysis in Δglo3 strains expressing the indicated Glo3 constructs. Cells were grown to mid-logarithmic phase and glucose starved for a period of 2 hours prior to FRAP measurement. The plot, reflecting the recovery of Arf1-GFP at Golgi membranes (Vrg4-mCherry), represents the mean FRAP curves with the fits.
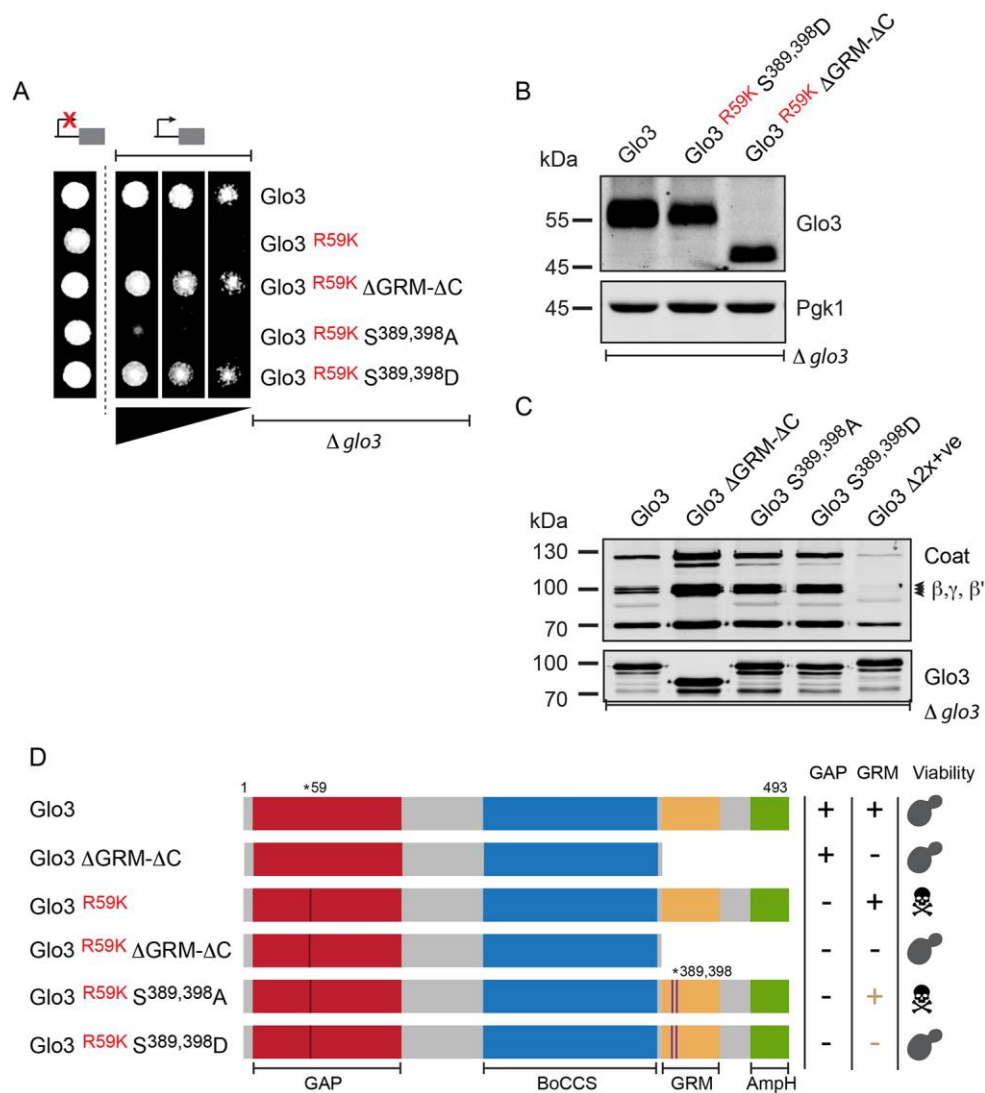
Fig. 5. Phosphorylation/dephosphorylation regulates Glo3 function

(A) Growth assay. Growth of Δ*glo3* strains harbouring the indicated constructs on synthetic dropout media was assayed in *MET25*-promoter repressing (high methionine; control indicated by scheme of a repressed promoter) and inducing (normal methionine; test indicated by scheme of an induced promoter) conditions. The phospho-mimetic mutant of the Glo3 motif rescues the dominant negative effect of the GAP-dead Glo3 indicating that phosphorylation/ dephosphorylation of the Glo3 motif regulates Glo3 function.

(B) Expression analysis of proteins in the indicated strains grown in Met25 promoter inducing (normal methionine; Test) conditions.

(C) Affinity chromatography of GFP-tagged Glo3 variants from detergent extracts of Δ*glo3* strains harbouring the indicated GFP-tagged constructs and subsequent evaluation of COPI association. Glo3 ΔGRM-ΔC – combined deletion of amphipathic helix and Glo3 motif; Glo3 S389,398A – alanine substitution of the indicated serines-non-phosphorylated mimetic; Glo3 S389,398A – aspartic acid substitution of the indicated serines- phosphomimetic. Glo3 Δ2x+ve – alanine substitution of COPI binding region.

(D) Summary. The Glo3 motif regulates the function of the GAP domain. Inactivation of the Glo3 motif by truncation or phosphorylation (phosphomimetic) rescues the dominant negative lethality caused by a non-functional GAP domain. Inferred functionality of the GRM domain is highlighted in brown. GTPase activating domain (GAP), Binding of Coatomer, Cargo and SNARE domain (BoCCS), Glo3 motif (GRM), amphipathic helix (AmpH).
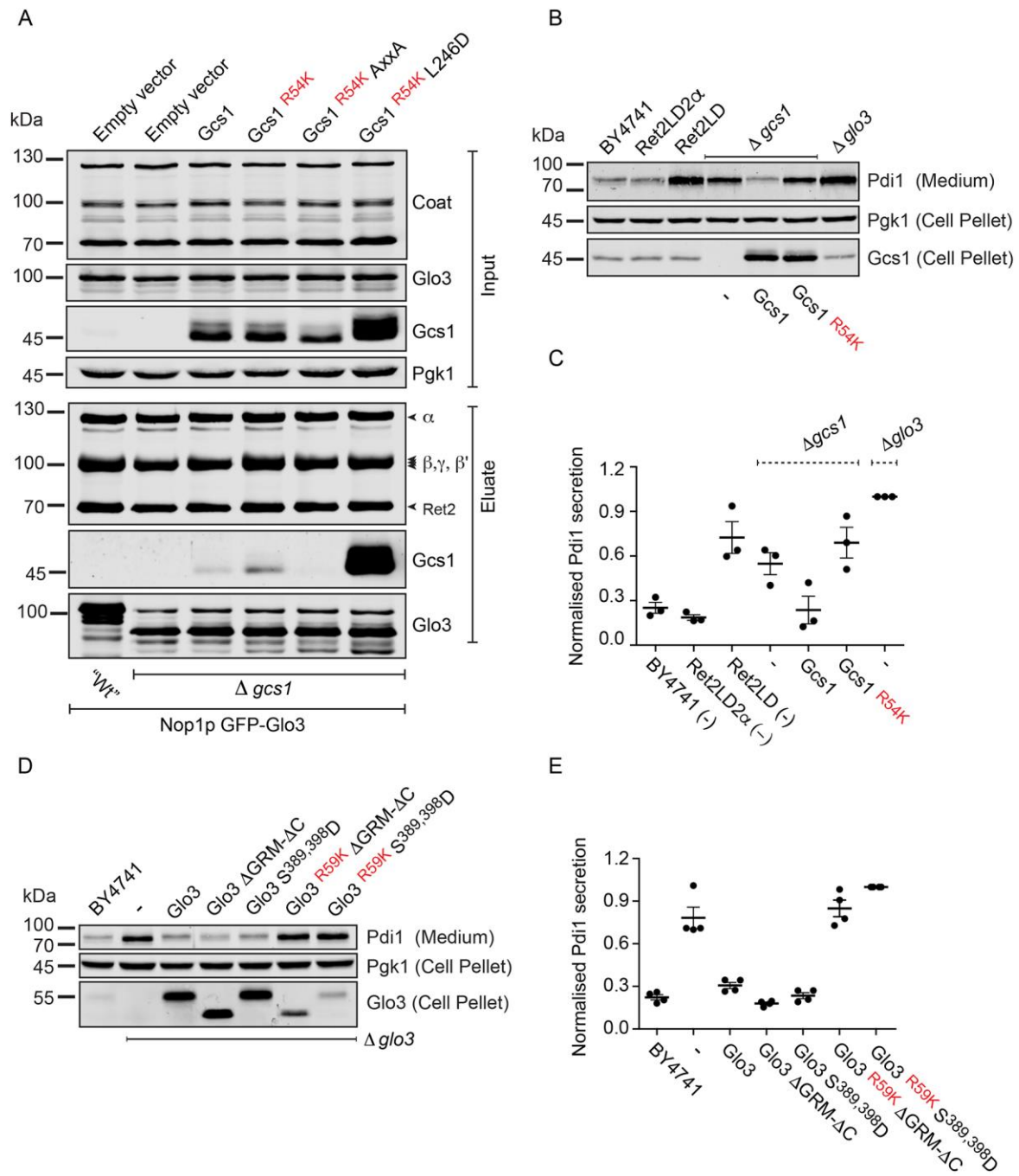
Fig. 6. Manipulating Gcs1 or COPI in the beta-Arf niche have similar effects on cargo sorting

(A) Affinity chromatography of GFP-tagged Glo3 from detergent extracts of Δ*gcs1* strains harbouring the indicated Gcs1 constructs and subsequent evaluation of COPI

and Gcs1 association. Gcs1 (R54K) – GAP-dead mutant of Gcs1; L246D – ALPS mutant; Gcs1 AxxA – alanine substitution of C-terminal tryptophan-based COPI recognition signal.

(B) Secretion assay of the indicated strains harbouring the indicated plasmids. Proteins secreted into the culture medium were analysed by SDS-PAGE and immunoblot analysis using antibodies specific for Pdi1. Cell pellets from the same cultures were also analysed using antibodies specific for Pgk1 and Gcs1.

(C) Plot of the relative amounts of Pdi1 secreted into the culture medium by the indicated strains, as quantified by the densiometric analysis of immunoblots. Quantification of three independent experiments. Error bars depict s.e.m.

(D) Secretion assay of the indicated strains harbouring the indicated plasmids. Proteins secreted into the culture medium were analysed by SDS-PAGE and immunoblot analysis using antibodies specific for Pdi1. Cell pellets from the same cultures were also analysed using antibodies specific for Pgk1 and Glo3.

(E) Plot of the relative amounts of Pdi1 secreted into the culture medium by the indicated strains, as quantified by the densiometric analysis of immunoblots. Quantification of four independent experiments. Error bars depict s.e.m.
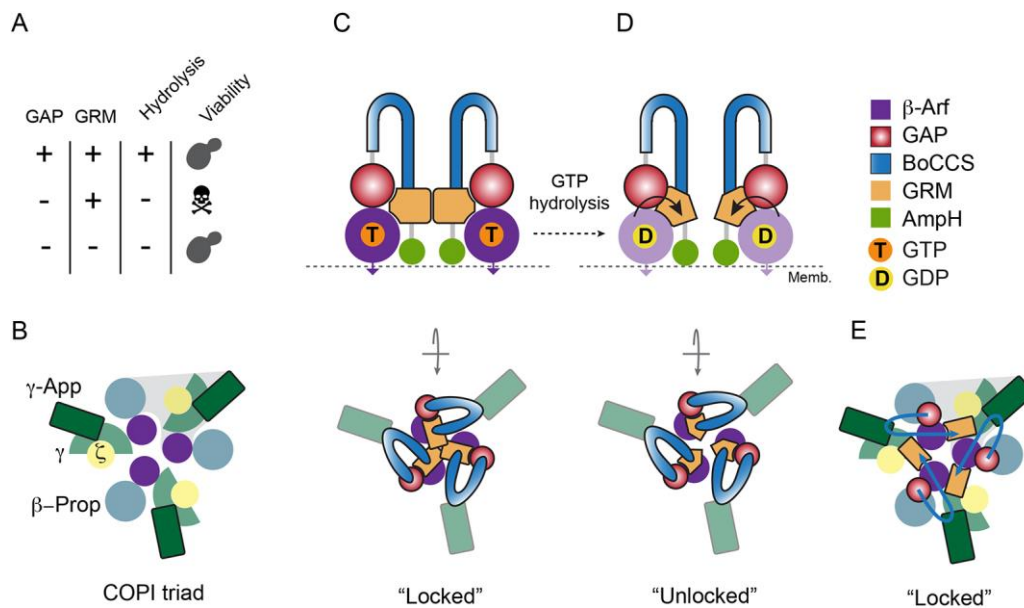
Fig. 7. The GRM domain regulates Glo3 function

(A) Table summarising the key results obtained by manipulating the GAP and the GRM domain.

(B) Model: Adjacent GRM domains interconnect individual coat molecules at the heart of the triad effectively locking the triad together and stabilising COPI on the membrane.

(C) Model: GTP hydrolysis in γ-Arf triggers a conformational change in the GRM domain and uncouples adjacent GRM domains effectively unlocking the triad and promoting the dissociation of COPI.

(D) Schematic illustration of the COPI triad for structural orientation.

(E) Model: The GRM domains of Glo3 interconnect individual coat molecules at the heart of the triad effectively locking the triad together and stabilizing COPI on the membrane. In this depiction, the GRM domain interconnects adjacent coat heptamers within a triad rather than adjacent GRM domains of neighboring Glo3 molecules

Table S1. Yeast strains used in this study

No.	Strain	Genotype	Source
1.	BY4741	*MATa his3Δ0 leu2Δ0 met15Δ0 ura3Δ0*	Arakel et al. 2016
2.	Ret2LD2α	*(BY4743 Spore) MATa his3Δ1 leu2Δ0 met15Δ0 ura3Δ0; YFR051c::kanMX4; p415 ret2LD2α*	Arakel et al. 2016
3.	Ret2LD	*(BY4743 Spore) MATa his3Δ1 leu2Δ0 met15Δ0 ura3Δ0; YFR051c::kanMX4; p415 ret2LD*	Arakel et al. 2016
4.	Δgcs1	*MATa his3Δ0 leu2Δ0 met15Δ0 ura3Δ0; YDL226C::CloNAT*	This study
5.	Δglo3	*MATa his3Δ0 leu2Δ0 met15Δ0 ura3Δ0; YER122C::CloNAT*	This study
		MATa his3-11,15 leu2, trp1, ura3, ade2 glo3::HIS3	Estrada et al., 2014
6.	GFP-Glo3	*MATa his3Δ0 leu2Δ0 met15Δ0 ura3Δ0; Nop1prom-GFP- YER122C:: ura3*	This study
7.	Δgcs1 GFP Glo3	*MATa his3Δ0 leu2Δ0 met15Δ0 ura3Δ0; YDL226C::CloNAT; Nop1prom-GFP-YER122C:: ura3*	This study
8.	sec26FW (F856A, W860A)	*MATa his3-11,15 leu2, trp1, ura3, ade2*	This study
9.	YAS4326 Snf1K84R-HA	*MATa Snf1::Snf1K84R-3HA(TRP) leu2,3, his 3-11, trp1-Δ1 ura3-1 ade2-1*	This study
10.	YAS3787 Δsnf1	*MATa Snf1::His3 leu2,3, his 3-11, trp1-Δ1 ura3-1 ade2-1*	This study
11.	YAS3098	*MATa Snf1:: Snf1-3HA(TRP) leu2,3, his 3-11, trp1-Δ1 ura3-1 ade2-1*	This study
12.	YAS4516	*MATa ARF1::ARF1-yEGFP (kanMX), VRG4::VRG4-mCherry (hphNTI) glo3::URA3 leu2-Δ1, lys2-801 ade2-101c his3-Δ200 p415 Glo3*	This study

Table S2. Plasmids used in this study

All plasmids used in this study from the Schwappach lab have been deposited with the Addgene plasmid repository. A detailed description of those plasmids is available at: https://www.addgene.org/Blanche_Schwappach/

No.	Plasmids	Addgene ID	Database ID
1.	p415 Gcs1	112646	AU2328
2.	p415 Gcs1 R54K	112647	AU2329
3.	p415 Gcs1 R54K L246D	112648	AU2330
4.	p415 Gcs1 R54K AxxA	112649	AU2331
5.	p415 Gcs1 Δ3xF AxxA	112650	AU2332
6.	p415 Glo3	112651	AU2333
7.	p415 Glo3 R59K	112652	AU2334
8.	p415 Glo3 R59K ΔC	112653	AU2335
9.	p415 Glo3 R59K ΔGRM-ΔC	112654	AU2336
10.	p415 Glo3 R59K Δ2x+ve	112655	AU2337
11.	p415 Glo3 R59K S389,398 A	112656	AU2338
12.	p415 Glo3 R59K S389,398 D	112657	AU2339
13.	p415 GFP-Glo3	112658	AU2340
14.	p415 GFP-Glo3 ΔGRM-ΔC	112659	AU2341
15.	p415 GFP-Glo3 S389,398 A	112660	AU2342
16.	p415 GFP-Glo3 S389,398 D	112661	AU2343
17.	p415 GFP-Glo3 Δ2x+ve	112662	AU2344
18.	p415 Met25 Glo3 ΔGRM-ΔC	129487	
19.	p415 Met25 Glo3 S389,398 A	129485	
20.	p415 Met25 Glo3 S389,398 D	129486	
21.	A102 GAP-BoCCS-GRM	123286	
22.	A102 GAP-BoCCS	123287	
23.	A102 BoCCS-GRM	123288	
24.	A102 par-BoCCS-GRM	123289	
25.	A102 BoCCS	123290	
26.	A102 GRM	123291	
27.	A102 Glo3 Δ AmpH Δ2x+ve	129484	
28.	p425TEF Glo3-FLAG		
29.	p425TEF Glo3-FLAG S389D		
30.	p425TEF Glo3-FLAG SS389/390AA		

Table S3. Proteins co-purifying with Glo3 and Gcs1.

List of complete protein identification results from LC-MS/MS analysis of affinity purified Glo3 and Gcs1. Contains spectral counts of identified proteins and their UniProt accession identities. See Excel file.

Click here to Download Table S3

Table S4. Arf1-GFP FRAP parameters.

Auxiliary to Fig. 4D and 4E.

Kinetic parameters derived from the FRAP data obtained by FRAP analysis of Arf1-GFP turnover at the Golgi. Mean with 95% confidence interval for dissociation rate k_{off} and mobile fraction F_m are shown.

Protein analyzed	Strain background	D	Dissociation rate k_{off} [s^{-1}]		Mobile fraction F_m [%]	
			mean	95% CI	mean	95% CI
Arf1 GFP	WT	+	0.164	0.154 to 0.173	0.769	0.761 to 0.776
	WT	-	0.234	0.219 to 0.249	0.854	0.849 to 0.859
	Δglo3 +EV	+	0.198	0.182 to 0.213	0.713	0.707 to 0.719
	Δglo3 +Glo3 WT	+	0.209	0.192 to 0.226	0.706	0.701 to 0.712
	Δglo3 +Glo3 AA	+	0.283	0.258 to 0.308	0.622	0.618 to 0.627
	Δglo3 +Glo3 DD	+	0.196	0.177 to 0.215	0.765	0.756 to 0.773

Calculated parameters derived from FRAP analysis of Arf1 GFP at the cis-Golgi compartment. CI – confidence interval. D – Glucose.

Table S5. Antibodies used in this study

Unique Identifier	Antibody	Species	Source
Ab0559	Coat (COPI)	Polyclonal	Rabbit	Hans Dieter Schmitt, MPI for Biophysical Chemistry, Germany
Ab0172	GFP	Polyclonal	Rabbit	Torrey Pines biolabs (TP401)
Ab0234	MBP	Monoclonal	Mouse	New England BioLabs (E8032S)
Ab0180	Glo3	Polyclonal	Rabbit	Anne Spang, Biozentrum University of Basel, Switzerland.
Ab0162	Gcs1	Polyclonal	Rabbit	Anne Spang, Biozentrum University of Basel, Switzerland.
Ab0270	Pgk1	Monoclonal	Mouse	Thermo Fisher Scientific (459250)

Supplementary figures:

Fig. S1. COPI binds the BoCCS domain of Glo3.

Related to Figure 2

Binding of TAP-purified coatomer to MBP fusion proteins of Glo3. The bound fraction was eluted and analysed by SDS/PAGE. Western blots were detected with a coat antiserum recognising five of the seven coatomer subunits. Glo3 Δ2x+ve – alanine substitution of COPI binding region within the BoCCS domain.
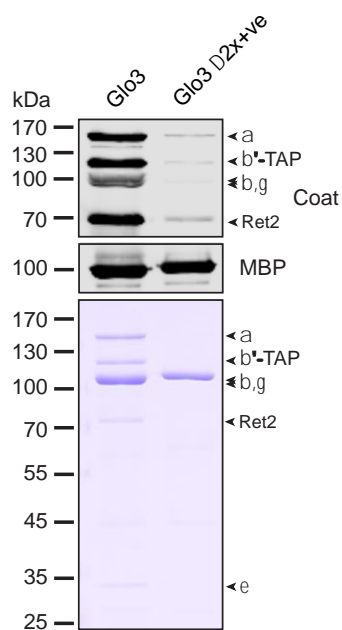
Fig. S2. Deletion of the Glo3 C-terminal amphipathic helix does not perturb its intracellular localization or its association with COPI.

Related to Figure 3

(A) Affinity chromatography of GFP-tagged Glo3 variants from detergent extracts of Δ*glo3* strains harbouring the indicated GFP-tagged constructs and subsequent evaluation of COPI association. Western blots were detected with a coat antiserum recognising five of the seven coatomer subunits.

(B) Steady-state localisation analysis of GFP tagged proteins (expressed under the *Met25* promoter) in a Δ*glo3* strain. Scale bar, 5 µm.
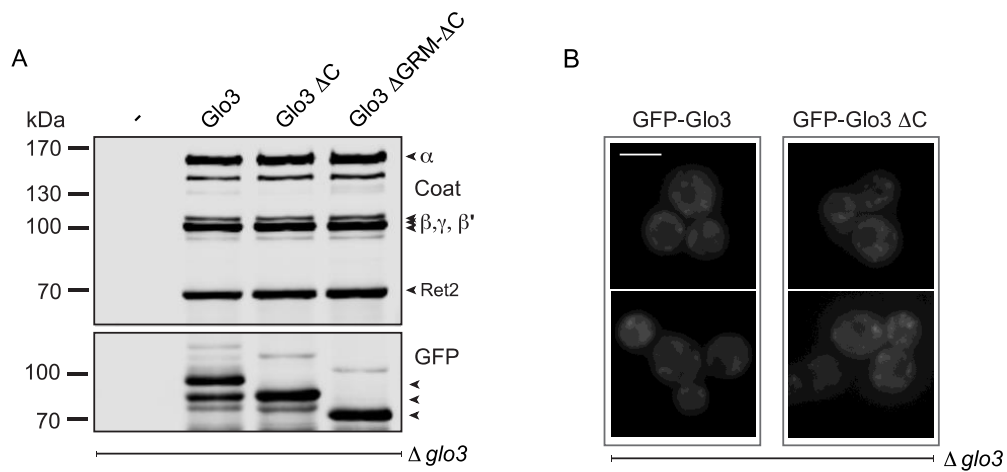
Fig. S3. S389 of the GRM domain is phosphorylated by the Snf1 Kinase. Related to Figure 4

(A) Schematic representation of the Glo3 variants used in (B and C).

(B) Immunoprecipitation of HA-tagged Snf1 for use in (C).

(C) Kinase assay demonstrating direct phosphorylation of Glo3 by Snf1. Purified Glo3 and variants thereof were incubated in the presence of Snf1, a kinase dead Snf1 mutant (K84R) or in its absence, subjected to SDS-PAGE and detected by autoradiography.

(D) Quantification of S389 phosphorylation in the presence or absence of the Snf1 kinase using a S398A construct.

(E) Quantification of S398 phosphorylation in the presence or absence of the Snf1 kinase using a S389A construct.

(F) Growth assay. Growth of *sec26^{FW}* *Δglo3* strains harbouring the indicated constructs.
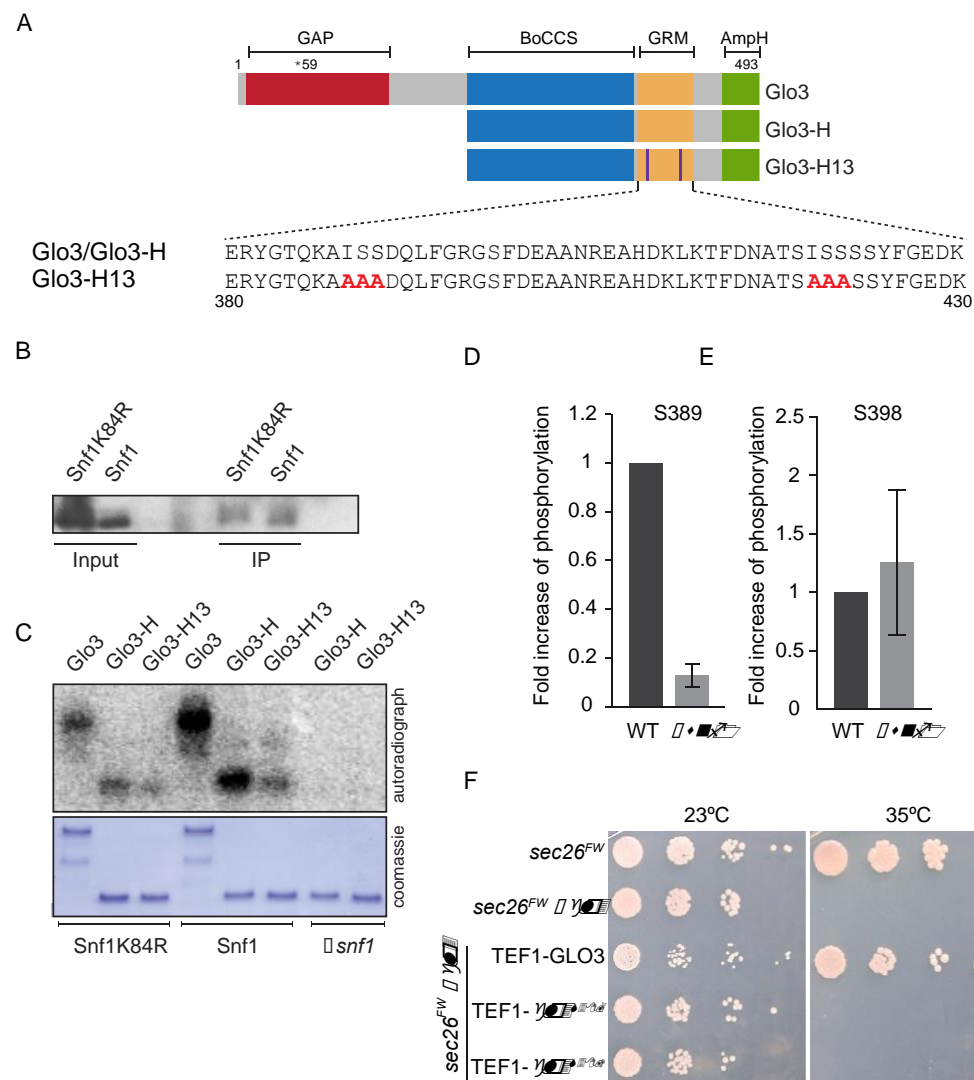
Fig S4. Phosphorylation/ dephosphorylation of the Glo3 GRM domain alters Arf1 dynamics on Golgi membranes.

Related to Figure 4

Live cell imaging of C-terminally GFP tagged Arf1 and C-terminally mCherry tagged Vrg4 in a Δ*glo3* strain expressing the indicated constructs. Arrows indicate fields/regions of co-localisation of Arf1 and the Golgi marker Vrg4 used for fluorescence recovery after photobleaching (FRAP) experiments to study the dynamics of Arf1 at the Golgi. Scale bar, 5 μm.
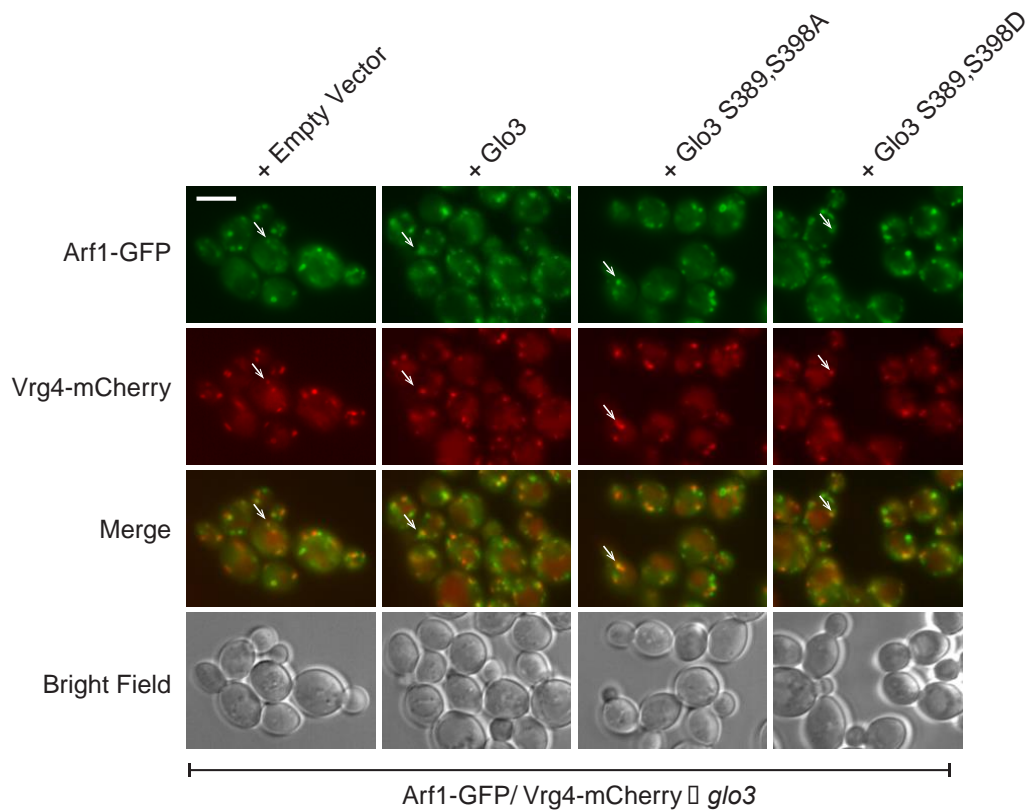
References:

1. Kettenbach AN, Gerber SA. Rapid and Reproducible Single-Stage Phosphopeptide Enrichment of Complex Peptide Mixtures: Application to General and Phosphotyrosine-Specific Phosphoproteomics Experiments. Analytical Chemistry. American Chemical Society; 2011;83: 7635–7644. doi:10.1021/ac201894j

2. Hindupur SK, Colombi M, Fuhs SR, Matter MS, Guri Y, Adam K, et al. The protein histidine phosphatase LHPP is a tumour suppressor. Nature. Nature Publishing Group; 2018;555: 678–682. doi:10.1038/nature26140

3. Ruiz A, Liu Y, Xu X, Carlson M. Heterotrimer-independent regulation of activation-loop phosphorylation of Snf1 protein kinase involves two protein phosphatases. Proc Natl Acad Sci U S A. National Academy of Sciences; 2012;109: 8652–8657. doi:10.1073/pnas.1206280109

4. Nicastro R, Tripodi F, Gaggini M, Castoldi A, Reghellin V, Nonnis S, et al. Snf1 Phosphorylates Adenylate Cyclase and Negatively Regulates Protein Kinase A-dependent Transcription in Saccharomyces cerevisiae. J Biol Chem. 2015;290: 24715–24726. doi:10.1074/jbc.M115.658005